JACS
JOURNAL OF THE AMERICAN CHEMICAL SOCIETY

Article

pubs.acs.org/JACS

Cysteinate Protonation and Water Hydrogen Bonding at the Active-Site of a Nickel Superoxide Dismutase Metallopeptide-Based Mimic: Implications for the Mechanism of Superoxide Reduction

Jason Shearer,* Kristy L. Peck, Jennifer C. Schmitt, and Kosh P. Neupane

Department of Chemistry, University of Nevada, Reno, Reno, Nevada 89557, United States

Supporting Information

ABSTRACT: Nickel-containing superoxide dismutase (NiSOD) is a mononuclear cysteinate-ligated nickel metalloenzyme that catalyzes the disproportionation of superoxide into dioxygen and hydrogen peroxide by cycling between Ni^{II} and Ni^{III} oxidation states. All of the ligating residues to nickel are found within the first six residues from the N-terminus, which has prompted several research groups to generate NiSOD metallopeptide-based mimics derived from the first several residues of the NiSOD sequence. To assess the viability of using these metallopeptide-based mimics (NiSOD maquettes) to probe the mechanism of SOD catalysis facilitated by NiSOD, we computationally explored the initial step of the O_2^- reduction mechanism catalyzed by the NiSOD maquette $\{Ni^{II}(SOD^{m1})\}$ (SOD^{m1} = HCDLP CGVYD PA). Herein we use spectroscopic (S K-edge X-ray absorption spectroscopy, electronic absorption spectroscopy, and circular dichroism spectroscopy) and computational techniques to derive the detailed active-site structure of $\{Ni^{II}(SOD^{m1})\}$. These studies suggest that the $\{Ni^{II}(SOD^{m1})\}$ active-site possesses a Ni^{II}-S(H^+)-Cys(6) moiety and at least one associated water molecule contained in a hydrogen-bonding interaction to the coordinated Cys(2) and Cys(6) sulfur atoms. A computationally derived mechanism for O_2^- reduction using the formulated active-site structure of $\{Ni^{II}(SOD^{m1})\}$ suggests that O_2^- reduction takes place through an apparent initial outersphere hydrogen atom transfer (HAT) from the Ni^{II}-S(H^+)-Cys(6) moiety to the O_2^- molecule. It is proposed that the water molecule aids in driving the reaction forward by lowering the Ni^{II}-S(H^+)-Cys(6) pK_a. Such a mechanism is not possible in NiSOD itself for structural reasons. These results therefore strongly suggest that maquettes derived from the primary sequence of NiSOD are mechanistically distinct from NiSOD itself despite the similarities in the structure and physical properties of the metalloenzyme vs the NiSOD metallopeptide-based models.

Superoxide (O_2^-) is a toxic reactive oxygen species (ROS) formed through the adventitious one electron reduction of dioxygen.[1,2] As it is an unavoidable byproduct of aerobic respiration organisms have developed pathways to degrade O_2^- before it can initiate extensive cellular damage.[2−7] The most prevalent O_2^- degradation enzymes are the superoxide dismutases (SODs).[2−6] These enzymes utilize redox active transition-metal cofactors to catalyze superoxide disproportionation through a highly efficient ping-pong type mechanism by accessing reduced (SOD^{red}) and oxidized (SOD^{ox}) redox states:

$$SOD^{red} + O_2^- + 2H^+ \rightarrow SOD^{ox} + H_2O_2 \quad (1a)$$

$$SOD^{ox} + O_2^- \rightarrow SOD^{red} + O_2 \quad (1b)$$

The most recently discovered SOD is nickel-containing superoxide dismutase (NiSOD), which is widely expressed by aquatic and soil bacteria.[4,5,8−12] As its name suggests, NiSOD contains a redox-active nickel cofactor at its active site and facilitates superoxide disproportionation by cycling between reduced Ni^{II} and oxidized Ni^{III} oxidation states. In its active form NiSOD is homohexameric with each monomer containing a mononuclear nickel ion. The nickel ion is situated at the bottom of a ∼15 Å long channel within an N-terminal loop structure (the so-called nickel binding hook).[13−15] The nickel binding hook has the consensus sequence HCXXPC and contains all of the residues required for nickel coordination.[11]

In the reduced form of NiSOD, the Ni^{II} ion is contained within a square-planar NiN_2S_2 coordination environment with ligands derived form the His(1) N-terminal amine nitrogen, the amidate nitrogen from Cys(2), and cysteinate sulfur atoms derived from Cys(2) and Cys(6) (Scheme 1). Oxidation to the Ni^{III} oxidation state yields a square-pyramidal coordination geometry about nickel following the coordination of the His(1) imidazole δ-nitrogen atom. O_2^- approaches the Ni-center from

Scheme 1

Received: August 3, 2014
Published: October 16, 2014

   dx.doi.org/10.1021/ja5079514 | J. Am. Chem. Soc. 2014, 136, 16009−16022

the surface through the 15 Å channel associating near the Ni center *trans* to the imidazole ligand.

We, and others, have utilized metallopeptides-based mimics derived from the NiSOD sequence (NiSOD maquettes) to explore the chemistry of NiSOD itself.[12,16−24] These NiSOD maquettes have been shown to replicate the geometric structure, electronic structure, and spectroscopic properties of NiSOD. Furthermore, these NiSOD maquettes are catalytically active, displaying high SOD activity with k_{cat} values approaching 6×10^8 M^{-1} s^{-1} for some metallopeptide-based models.[12]

We have utilized a family of NiSOD maquettes derived from the first 12 residues of the *Streptomyces coelicolor* NiSOD sequence, the {Ni(SOD^{m1})} family (SOD^{m1} = HCDLP-CGVYD-PA; Chart 1).[16−18,20,21] These SOD active metallopeptides have proven useful in correlating different functional and structural aspects of NiSOD with its sequence. In one study the mechanism of O_2^- disproportionation catalyzed by {Ni(SOD^{m1}H(1)H^{Me})} was probed.[16] {Ni(SOD^{m1}H(1)H^{Me})} is a derivative of the parent {Ni(SOD^{m1})} metallopeptide that contains an *N*-methyl histidine (H^{Me}) in place of His(1) (SOD^{m1}H(1)H^{Me} = H^{Me}CDLP-CGVYD-PA). In that study O_2^- reduction facilitated by reduced {Ni^{II}(SOD^{m1}H(1)H^{Me})} was proposed to proceed through a proton-coupled electron-transfer (PCET) reaction with a significant quantum mechanical tunneling component. This was evidenced by a large room temperature solvent H/D kinetic isotope effect (KIE, ∼20) and the resulting Arrhenius activation parameters (virtually barrierless reaction). Considering the similarities in the reduced structures and disproportionation kinetics of {Ni^{II}(SOD^{m1}H(1)H^{Me})} vs other members of the {Ni^{II}(SOD^{m1})} family it is a reasonable supposition that the O_2^- reduction mechanism occurs via a nearly identical process among the {Ni^{II}(SOD^{m1})} family.

Chart 1. Active Site Structures of the Metallopeptides from the {Ni(SOD^{m1})} Family

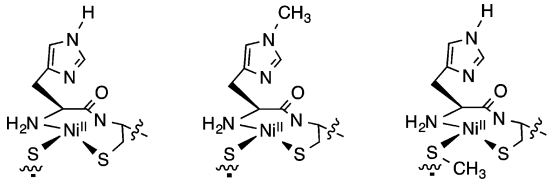

Spectroscopic studies suggested that the transferred "H•" (proton and electron) within {Ni^{II}(SOD^{m1}H(1)H^{Me})} originates from a protonated coordinated Ni^{II}-S(H$^+$)-Cys moiety. High vs low pH S K-edge X-ray absorption spectroscopy performed on {Ni^{II}(SOD^{m1}H(1)H^{Me})} was most insightful in formulating the Ni^{II}-S(H$^+$)-Cys moiety. In transition-metal complexes containing at least one hole in the nd-set a prominent peak in the pre-edge region of the S K-edge X-ray absorption corresponding to a thiolate S(1s) → Ψ_1* transition is typically observed (Ψ_1* corresponds to the lowest-energy acceptor state(s), which is typically metal nd in character).[25−27] The S K-edge X-ray absorption spectrum of {Ni^{II}(SOD^{m1}H(1)H^{Me})} obtained at pH 8.0 displayed no prominent pre-edge feature corresponding to a thiolate S(1s) → Ψ_1* transition. Furthermore, the edge was significantly broader than is typically observed for Ni^{II}-thiolates. The pH 8.0 S K-edge X-ray absorption spectrum obtained for {Ni^{II}(SOD^{m1}H(1)H^{Me})} was in fact similar to what would be predicted for Ni^{II}-thioether complexes,[28] which was suggestive that {Ni^{II}(SOD^{m1}H(1)H^{Me})} contained a Ni^{II}-S(H$^+$)-Cys moiety. Variable pH studies supported this notion; at pH 9.5, where the Ni^{II}-S(H$^+$)-Cys moiety would become deprotonated, the pre-edge feature corresponding to the thiolate S(1s) → Ψ_1* transition in the S K-edge X-ray absorption spectrum of {Ni^{II}(SOD^{m1}H(1)H^{Me})} appeared. Solomon and co-workers have demonstrated that reduced NiSOD likely contains a Ni^{II}-S(H$^+$)-Cys moiety as well.[28] Furthermore, metric parameters and spectroscopic signatures of reduced NiSOD and the maquettes are similar to one another. Taken together this suggests similar reduced active-site structures for the metalloenzyme vs the NiSOD maquette.

In this study we further probe the O_2^- reduction mechanism facilitated by these NiSOD maquettes. Herein we present the preparation of an *S*-methylated derivative of {Ni^{II}(SOD^{m1})}, {Ni^{II}(SOD^{m1}C(6)C^{Me})} (C^{Me} = *S*-methylcysteine; Chart 1). {Ni^{II}(SOD^{m1}C(6)C^{Me})} was utilized to aid in identifying the cysteinate sulfur atom that comprises the Ni^{II}-S(H$^+$)-Cys moiety within the parent metallopeptide. To better quantify the active-site structures of both {Ni^{II}(SOD^{m1}C(6)C^{Me})} and {Ni^{II}(SOD^{m1})}, detailed spectroscopic and computational studies of {Ni^{II}(SOD^{m1}C(6)C^{Me})} and {Ni^{II}(SOD^{m1})} under high and low pH were undertaken. These results yielded a detailed active-site structure of the catalytically active form of {Ni^{II}(SOD^{m1})}. The resulting structure of active {Ni^{II}(SOD^{m1})} was then used to provide accurate computational models to examine the mechanism of O_2^- reduction facilitated by the metallopeptide. The results presented in this study strongly suggest that, although NiSOD and {Ni^{II}(SOD^{m1})} likely have similar active-site structures, the mechanisms by which the two systems facilitate SOD catalysis are distinct.

RESULTS AND ANALYSIS

***S*-Methylcysteine Peptide Metalation and Nickel Binding.** To approximate the influence of a protonated coordinated cysteinate ligand on the active-site of {Ni^{II}(SOD^{m1})}, a series of Cys methylated derivatives of SOD^{m1} were prepared. Attempts to coordinate Ni^{II} to either the Cys(2)Cys^{Me} (H$_2$N-HC^{Me}DLP-CGVYD-PA-COOH; Cys^{Me} = *S*-methylcysteine) or Cys(2/6)Cys^{Me} (H$_2$N-HC^{Me}DLP-C^{Me}GVYD-PA-COOH) derivatives were unsuccessful. Over the pH range of 7.0 to 9.0 no evidence for Ni^{II} incorporation into the peptides was noted.

In contrast, Ni^{II} will readily bind to the Cys(6)Cys^{Me} derivative (SOD^{m1}C(6)C^{Me}; H$_2$N-HCDLP-C^{Me}GVYD-PA-COOH) forming {Ni^{II}(SOD^{m1}C(6)C^{Me})}. Solutions of {Ni^{II}(SOD^{m1}C(6)C^{Me})} in *N*-ethylmorpholine (NEM) buffer (50 mM NEM; pH 7.4) are reminiscent of the pH 7.4 solution of {Ni^{II}(SOD^{m1})}. Solutions of both metallopeptides are light pinkish beige in color.[17] However, unlike solutions of {Ni^{II}(SOD^{m1})}, which display a color change as the pH is elevated (pinkish beige to reddish brown),[18] solutions of {Ni^{II}(SOD^{m1}C(6)C^{Me})} do not change color over the pH range of 7.0−9.5. We also note that unlike {Ni^{II}(SOD^{m1})},[17] {Ni^{II}(SOD^{m1}C(6)C^{Me})} displayed no apparent redox activity over the range of −0.2 to 1.0 V vs SHE as determined by cyclic voltammetry and attempts to trap a Ni^{III} species following chemical oxidation. It therefore appears that the Ni^{III} oxidation state is not accessible over the range relevant for SOD catalysis. Thus, it is not surprising that {Ni^{II}(SOD^{m1}C(6)C^{Me})} is SOD inactive.

dx.doi.org/10.1021/ja5079514 | J. Am. Chem. Soc. 2014, 136, 16009−16022

The pH 7.4 Ni^{II} binding constant to $SOD^{m1}C(6)C^{Me}$ was determined spectrophotometrically using glycine as a competitive Ni^{II} chelating agent. These titrations yielded a Ni^{II} K_d value from $SOD^{m1}C(6)C^{Me}$ of 3(1) μM at pH 7.4. This Ni^{II} dissociation constant compares well with other K_d values we have previously measured for NiSOD maquettes.[17,19] Thus, the $Cys(6)Cys^{Me}$ modification is not having a major impact on Ni^{II} binding to the peptide in comparison to the parent unmodified peptide.

The geometry about the Ni^{II} center of $\{Ni^{II}(SOD^{m1}C(6)C^{Me})\}$ was probed by Ni K-edge X-ray absorption spectroscopy (Figure 1). The XANES region of the Ni K-edge X-ray

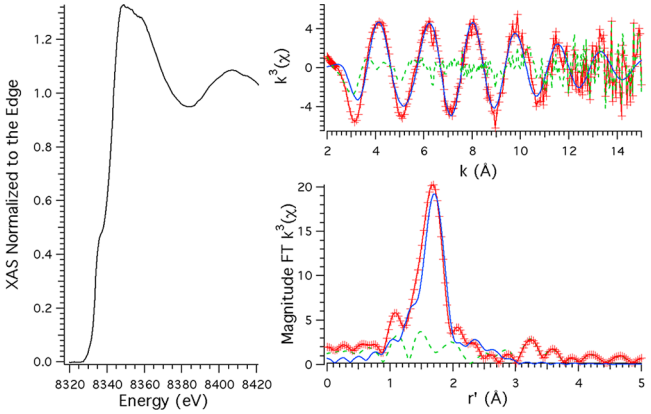

Figure 1. Nickel K-edge X-ray absorption spectrum of $\{Ni^{II}(SOD^{m1}C(6)C^{Me})\}$. The left spectrum depicts the XANES region of the Ni K-edge X-ray absorption spectrum. The top right spectrum depicts the unfiltered k^3 EXAFS spectrum (red spectrum), the simulation to the data (blue spectrum), and the difference spectrum between the experimental and simulated spectrum (green dashed spectrum). The bottom right spectrum depicts the magnitude Fourier transformed k^3 EXAFS spectrum (red spectrum), the simulation to the data (blue spectrum), and the difference spectrum between the experimental and simulated spectrum (green dashed spectrum). Simulation parameters: E_o = 8341.2 eV; shell no. 1: Ni−S, n = 2, r = 2.194(5) Å, σ = 0.006(1) Å ^{2}; shell no. 2: Ni−N, n = 2, r = 1.913(3) Å, σ = 0.006(1) Å ^{2}; ε^2 = 1.08.

absorption spectrum displays a small feature at 8331.8(2) eV (area = 0.02(1) eV relative to the edge) corresponding to the Ni(1s → 3d) transition and a more intense shoulder at 8337.7(1) eV (area = 0.41(1) eV relative to the edge) corresponding to the Ni(1s → $4p_z$) transition. Both of these features are consistent with square-planar Ni^{II}.[29] The EXAFS data are consistent with a four coordinate NiN_2S_2 complex. The best fit to the $\{Ni^{II}(SOD^{m1}C(6)C^{Me})\}$ EXAFS data yielded two Ni−N scatterers at 1.91 Å and two Ni−S scatterer at 2.19 Å (Chart 1, Table 1).[30]

Computational Models for $\{Ni^{II}(SOD^{m1}C(6)C^{Me})\}$ and $\{Ni^{II}(SOD^{m1})\}$ in Different Protonation States. Computational models for the active-sites of these metallopeptides were generated by approximating the reduced NiSOD active-site as a Ni(II) center coordinated to a 2-amino-*N*-(2-mercaptoethyl)-acetamidate ligand and an ethanethiolate coordinated to nickel *trans* to the amidate nitrogen ($(Ni^{II}(SOD))^-$). The ethanethiolate was then either methylated, generating Ni^{II}(SOD-Cys(6)Me), or protonated, generating $Ni^{II}(SOD\text{-}Cys(6)H^+)$.[31] In addition, a computational model was constructed with a water molecule hydrogen bonded to the cysteinate sulfur atoms ($Ni^{II}(SODCys(6)H^+)\cdots H_2O$). Geometry optimized structures were obtained using closed-shell restricted density functional theory (DFT, S = 0) using the BP86 functional with the def2-tzvp basis set and the COSMO solvation model with parameters applicable to water (Figure 2, Table 1).[32] We note that $Ni^{II}(SOD\text{-}Cys(6)H^+)$ is thermodynamically more stable than Cys(2) protonated $Ni^{II}(SOD\text{-}Cys(2)H^+)$ (ΔG = −4.5 kcal mol^{-1}).

The computationally derived structure of unprotonated $(Ni(SOD))^-$ displays Ni−S bond lengths of 2.178 (*trans*-amine) and 2.235 Å (*trans*-amidate) and Ni−N bond lengths of 1.972 (amine) and 1.889 Å (amidate). Although the average Ni−N bond length is consistent with the structural data for both $\{Ni^{II}(SOD^{m1})\}$ (pH 7.4) and NiSOD itself, the average calculated Ni−S bond length is longer than the experimentally determined Ni−S bond lengths for these systems (2.21 Å (calcd) vs 2.18 Å (exp.), Table 1). Instead, the average calculated Ni−S bond length matches the EXAFS derived average Ni−S bond length for $\{Ni^{II}(SOD^{m1}H(1)H^{Me})\}$ previously recorded at pH 9.5.[16]

The Cys(6) *S*-methylated computational model Ni^{II}(SOD-Cys(6)Me) possesses a Ni(II)−$S^{thiolate}$ bond length of 2.172 Å, a Ni(II)−$S^{thioether}$ bond length of 2.208 Å, a Ni(II)−N^{amine} bond length of 1.996 Å, and a Ni(II)−N^{amide} bond length of 1.864 Å (Table 1). The resulting average Ni−S and Ni−N bond lengths calculated for Ni^{II}(SOD-Cys(6)Me) therefore match those obtained experimentally for $\{Ni^{II}(SOD^{m1}C(6)C^{Me})\}$. An important structural aspect of Cys(6) methylation revealed by these computational models is the contraction of the Ni−S bond *trans* to the amide in Ni^{II}(SOD-Cys(6)Me) relative to $(Ni^{II}(SOD))^-$ by 0.027 Å. This is due to the relief of repulsive filled/filled Ni(3dπ)−S(3p) interactions between the metal center and the ligand upon methylation.[33−36]

Not only does the *trans*-amidate Ni−S bond contract upon methylation of the thiolate ligand, but it also contracts upon protonation relative to the *trans*-amidate Ni−S bond found in $(Ni^{II}(SOD))^-$. Upon protonation of the Cys(6) sulfur atom the Ni−S bond contracts by 0.03 Å relative to $(Ni^{II}(SOD))^-$ (2.205 Å) without effecting a dramatic change on the other Ni−S bond length. Furthermore, the average Ni−S bond length obtained for $Ni^{II}(SODCys(6)H^+)$ (2.19 Å) more closely matches the experimentally derived average pH 7.4 Ni−S bond length obtained for $\{Ni^{II}(SOD^{m1})\}$ (2.18 Å).

Table 1. Selected Bond Lengths (in Å) for Computational Models (BP86/def2-tzvp), $\{Ni^{II}(SOD^{m1})\}$ (Ni K-edge EXAFS), and $\{Ni^{II}(SOD^{m1}C(6)C^{Me})\}$ (Ni K-edge EXAFS)

	Ni^{II}(SOD-C(6)C^{Me})	Ni^{II}(SOD-C(6)H^+)	$Ni^{II}(SOD\text{-}C(6)H^+)\cdots H_2O$	$(Ni^{II}(SOD))^-$	$\{Ni^{II}(SOD^{m1})\}$ pH 7.4[a]	$\{Ni^{II}(SOD^{m1}C(6)C^{Me})\}$
Ni−S(1)[b]	2.172	2.174	2.175	2.178	2.18[c]	2.19[c]
Ni−S(2)[d]	2.208	2.205	2.190	2.235	–	–
Ni−N(1)[e]	1.996	1.995	1.992	1.972	1.91[c]	1.91[c]
Ni−N(2)[f]	1.864	1.858	1.862	1.889	–	–

[a]Refs 17 and 20. [b]*trans*-amine. [c]EXAFS derived average Ni−S bond length. [d]*trans*-amidate. [e]Amine nitrogen atom. [f]Amidate nitrogen atom.

dx.doi.org/10.1021/ja5079514 | J. Am. Chem. Soc. 2014, 136, 16009−16022

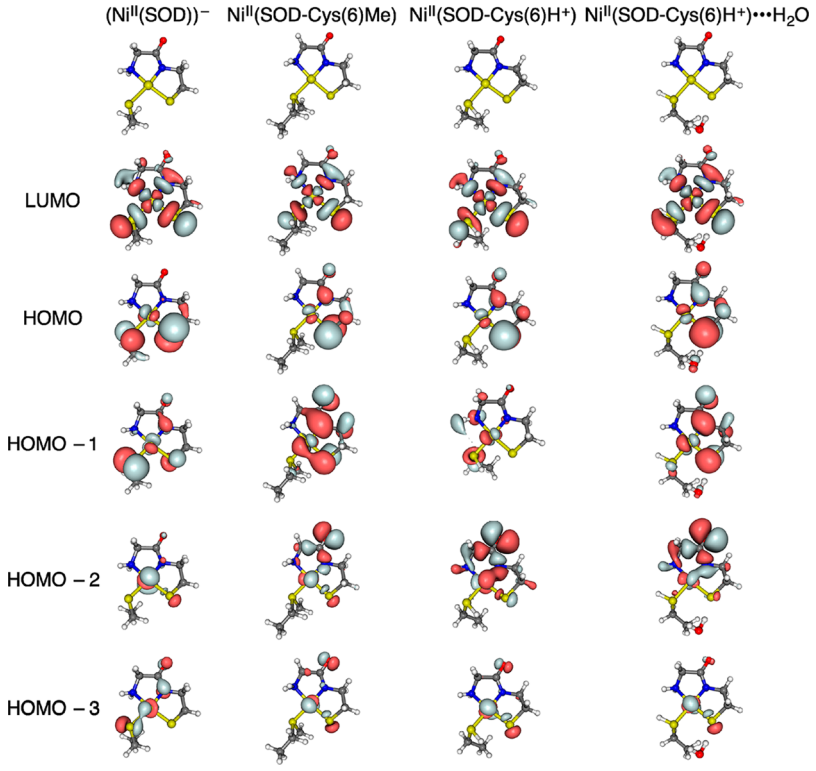

Figure 2. Geometry optimized models (top; BP86/def2-tzvp) and HOMO−3 through LUMO (PBE0/def2-tzvp) for $(Ni^{II}(SOD))^-$, Ni^{II}(SOD-Cys(6)Me), Ni^{II}(SOD-Cys(6)H^+), and Ni^{II}(SOD-Cys(6)H^+)···H_2O.

Addition of a water molecule contained in a hydrogen-bonding interaction to the cysteinates (Ni^{II}(SODCys(6)H^+)···H_2O) yielded a further shortening of the Ni−S bond *trans* to the amidate nitrogen, resulting in an average Ni−S bond length of 2.18 Å. The average Ni−S bond length matches the previously reported EXAFS data for {$Ni^{II}(SOD^{m1})$} at pH 7.4. Furthermore, the Ni ligand bond lengths also match the EXAFS[37] and crystallographically[14,15] derived bond lengths of NiSOD itself. We note that the addition of a water molecule also reorients the S−H^+ moiety such that the proton is positioned within the Cys(6)S−Ni−N^{amine} cleft. This structural aspect will become important for the proposed O_2^- reduction mechanism.

The average Ni−S bond lengths of Ni^{II}(SODCys(2)H^+) and Ni^{II}(SODCys(2)H^+)···H_2O (2.21 and 2.20 Å) are long relative to the EXAFS data obtained for {$Ni^{II}(SOD^{m1})$}. This is due to an elongated Ni−S bond *trans* to the amidate (2.247 Å) that is not substantially shortened upon Cys(6)S···H_2O hydrogen bonding. Taken together these data seem to suggest that at pH 7.4 {$Ni^{II}(SOD^{m1})$} possesses a Cys(6) sulfur atom that is protonated and that there is likely at least one water molecule associated hydrogen bonded to the Cys(2) and Cys(6) sulfur atoms. This formulation is supported by S K-edge X-ray absorption spectroscopy (see next section).

Isosurface plots for the LUMO through HOMO−3 for Ni^{II}(SOD-Cys(6)Me), Ni^{II}(SOD-Cys(6)H^+), Ni^{II}(SOD-Cys(6)H^+)···H_2O, and $(Ni^{II}(SOD))^-$ are displayed in Figure 2. The atomic orbital populations for the LUMO+1 through HOMO−4 for these computational models are displayed in Table 2 (PBE0/def2-tzvp). The LUMO through HOMO−3 calculated for $(Ni^{II}(SOD))^-$ are in line with what has been previously reported.[18,39] The unoccupied LUMO is best described as a Ni($3d_{x^2-y^2}$)-N/S(σ^*) antibonding orbital. The doubly occupied HOMO and HOMO−1 are S($3\pi^*$)-Ni($3d\pi$) and S(3π)-Ni($3d\pi$) antibonding orbitals. Next in energy is the Ni($3d_{z^2}$)-S(3σ) HOMO−2 followed by the Ni($3d_{xy}$)+S(3p)-Ni(2p) HOMO−3.

Ni^{II}(SOD-Cys(6)Me) and Ni^{II}(SOD-Cys(6)H^+) are electronically similar to one another. Upon protonation or methylation the Ni($3d_{x^2-y^2}$) LUMO and the Ni($3d_{z^2}$) HOMO−2 remain relatively unchanged compared to the MOs for $(Ni^{II}(SOD))^-$ with perturbations to their absolute energies and the Ni-ligand character to the MOs, which reflects the differential bonding in the three computational models. These perturbations include a reduction in ligand character and an increase in Ni character to the LUMO of Ni^{II}(SOD-Cys(6)H^+/Me) relative to $(Ni^{II}(SOD))^-$, which reflects the reduction in ligand-Ni covalency to this MO. The HOMO−2, in contrast, contains more ligand character from the amine and amide moieties. Furthermore, although the HOMO−2 remains primarily Ni($3d_{z^2}$) in character, it now contains significant contributions from the Ni($3d_{xy}$) orbital (the Ni(3d) orbital is ∼60% Ni($3d_{z^2}$) and ∼40% Ni($3d_{xy}$)). In addition, the amide oxygen and nitrogen atomic orbitals that participate in bonding are rotated in the HOMO−2 for Ni^{II}(SOD-Cys(6)H^+/Me) relative to $(Ni^{II}(SOD))^-$. In $(Ni^{II}(SOD))^-$ the amide oxygen is perpendicular to the *xy* plane resulting in a π-type interaction with the Ni(3d) orbital, while in Ni^{II}(SOD-Cys(6)H^+/Me) the orbitals are contained within the *xy* plane resulting in a σ-type interaction with the Ni(3d) orbital. More substantial changes observed for these two computational models with respect to $(Ni^{II}(SOD))^-$ are found in the doubly filled orbitals resulting from Ni($3d\pi$)−S(3π) interactions (the HOMO, HOMO−1, and HOMO−3). This is a result of the unavailability of the Cys(6)-S($3p_x$) orbital for π-bonding to the nickel center upon protonation or methylation. The HOMO of Ni^{II}(SOD-

dx.doi.org/10.1021/ja5079514 | J. Am. Chem. Soc. 2014, 136, 16009−16022

Table 2. Orbital Energy (normalized to the HOMO) and Atomic Orbitals Composition of Cys(6) Methylated, Cys(6) and Cys(2) Protonated, and Unprotonated NiSOD Computational Models[a]

orbital	$(Ni^{II}(SOD))^{-}$	$Ni^{II}(SOD\text{-}C(6)C^{Me})$	$Ni^{II}(SOD\text{-}C(6)H^{+})$	$Ni^{II}(SOD\text{-}C(6)H^{+})\cdots H_2O$
LUMO+1	energy: 5.08 eV	energy: 4.99 eV	energy: 4.64 eV	energy: 5.40 eV
	Ni 3d: 6.1%	Ni 3d: 6.7%	Ni 3d: 5.6%	Ni 3d: 4.2%
	S(a) 3p: 2.1%	S(a) 3p: 17.6%	S(a) 3p: 18.0%	S(a) 3p: 20.7%
	S(b) 3p: 0.3%	S(b) 3p: 1.1%	S(b) 3p: 1.9%	S(b) 3p: 0.8%
	N(a) 2p: 1.2%	N(a) 2p: 0.2%	N(a) 2p: 0.1%	N(a) 2p: 0.3%
	N(b) 2p: 2.1%	N(b) 2p: 1.6%	N(b) 2p: 1.6%	N(b) 2p: 1.4%
	O 2p: 0.8%	O 2p: 0.4%	O 2p: 0.2%	O 2p: 0.0%
LUMO	energy: 4.45 eV	energy: 4.13 eV	energy: 4.11 eV	energy: 4.17 eV
	Ni 3d: 41.7%	Ni 3d: 52.4%	Ni 3d: 51.9%	Ni 3d: 42.8%
	S(a) 3p: 16.4%	S(a) 3p: 5.2%	S(a) 3p: 5.2%	S(a) 3p: 14.5%
	S(b) 3p: 28.2%	S(b) 3p: 13.0%	S(b) 3p: 13.4%	S(b) 3p: 23.2%
	N(a) 2p: 3.3%	N(a) 2p: 4.5%	N(a) 2p: 5.5%	N(a) 2p: 5.5%
	N(b) 2p: 2.6%	N(b) 2p: 3.0%	N(b) 2p: 2.9%	N(b) 2p: 3.1%
	O 2p: 0.4%	O 2p: 0.9%	O 2p: 0.8%	O 2p: 0.9%
HOMO	energy: 0 eV	energy: 0 eV	energy: 0 eV	energy: 0 eV
	Ni 3d: 19.5%	Ni 3d: 13.0%	Ni 3d: 16.1%	Ni 3d: 17.1%
	S(a) 3p: 16.4%	S(a) 3p: 0.1%	S(a) 3p: 0.3%	S(a) 3p: 0.0%
	S(b) 3p: 52.1%	S(b) 3p: 57.3%	S(b) 3p: 56.8%	S(b) 3p: 49.4%
	N(a) 2p: 0.4%	N(a) 2p: 7.8%	N(a) 2p: 7.7%	N(a) 2p: 10.5%
	N(b) 2p: 0.3%	N(b) 2p: 0.0%	N(b) 2p: 0.0%	N(b) 2p: 0.0%
	O 2p: 0.2%	O 2p: 4.2%	O 2p: 4.5%	O 2p: 6.1%
HOMO−1	energy: −0.17 eV	energy: −0.62 eV	energy: −0.63 eV	energy: −0.51 eV
	Ni 3d: 26.0%	Ni 3d: 20.3%	Ni 3d: 20.9%	Ni 3d: 21.3%
	S(a) 3p: 40.4%	S(a) 3p: 0.2%	S(a) 3p: 0.1%	S(a) 3p: 16.7%
	S(b) 3p: 1.5%	S(b) 3p: 12.1%	S(b) 3p: 13.0%	S(b) 3p: 0.6%
	N(a) 2p: 1.8%	N(a) 2p: 25.6%	N(a) 2p: 25.8%	N(a) 2p: 16.9%
	N(b) 2p: 0.5%	N(b) 2p: 0.3%	N(b) 2p: 0.2%	N(b) 2p: 6.1%
	O 2p: 2.6%	O 2p: 17.9%	O 2p: 17.3%	O 2p: 16.0%
HOMO−2	energy: −0.84 eV	energy: −0.92 eV	energy: −0.95 eV	energy: −1.02 eV
	Ni 3d: 75.2%	Ni 3d: 57.5%	Ni 3d: 48.1%	Ni 3d: 55.8%
	S(a) 3p: 2.3%	S(a) 3p: 0.8%	S(a) 3p: 0.5%	S(a) 3p: 0.6%
	S(b) 3p: 8.0%	S(b) 3p: 5.6%	S(b) 3p: 0.2%	S(b) 3p: 1.1%
	N(a) 2p: 2.2%	N(a) 2p: 4.7%	N(a) 2p: 26.0%	N(a) 2p: 9.9%
	N(b) 2p: 0.5%	N(b) 2p: 0.6%	N(b) 2p: 11.6%	N(b) 2p: 0.6%
	O 2p: 1.1%	O 2p: 15.5%	O 2p: 15.4%	O 2p: 11.0%
HOMO−3	energy: −0.90 eV	energy: −1.24 eV	energy: −1.25 eV	energy: −1.15 eV
	Ni 3d: 35.2%	Ni 3d: 50.5%	Ni 3d: 56.8%	Ni 3d: 60.0%
	S(a) 3p: 18.8%	S(a) 3p: 1.1%	S(a) 3p: 1.5%	S(a) 3p: 2.1%
	S(b) 3p: 3.7%	S(b) 3p: 13.6%	S(b) 3p: 16.1%	S(b) 3p: 17.9%
	N(a) 2p: 14.2%	N(a) 2p: 1.7%	N(a) 2p: 1.6%	N(a) 2p: 1.5%
	N(b) 2p: 1.1%	N(b) 2p: 0.5%	N(b) 2p: 0.4%	N(b) 2p: 0.4%
	O 2p: 9.5%	O 2p: 16.9%	O 2p: 8.4%	O 2p: 2.6%
HOMO−4	energy: −1.43 eV	energy: −1.61 eV	energy: −1.71 eV	energy: −1.65 eV
	Ni 3d: 6.8%	Ni 3d: 40.0%	Ni 3d: 45.5%	Ni 3d: 36.0%
	S(a) 3p: 2.1%	S(a) 3p: 3.1%	S(a) 3p: 0.7%	S(a) 3p: 0.1%
	S(b) 3p: 0.3%	S(b) 3p: 33.3%	S(b) 3p: 39.6%	S(b) 3p: 36.2%
	N(a) 2p: 1.2%	N(a) 2p: 0.0%	N(a) 2p: 0.0%	N(a) 2p: 0.1%
	N(b) 2p: 3.5%	N(b) 2p: 4.6%	N(b) 2p: 4.7%	N(b) 2p: 4.6%
	O 2p: 0.8%	O 2p: 0.3%	O 2p: 0.2%	O 2p: 0.2%

[a]All orbital compositions were derived from a Lowden population analysis of the PBE0/def2-tzvp single point calculations. S(a) *trans*-amine; S(b) *trans*-amide; N(a) amide; N(b) amine.

Cys(6)Me/H^+) becomes primarily S/N(π)-Ni(3dπ) antibonding in character. Similarly, the HOMO−3 becomes a predominantly S/N(π)-Ni($3d_{xy}/3d_{z^2}$) antibonding orbital. The one major difference between the two computational models is the HOMO−1. For Ni^{II}(SOD-Cys(6)Me) the HOMO−1 is derived from a Cys(2)S/N^{amide}(π)−Ni(3dπ) antibonding interaction, while the HOMO−1 for Ni^{II}(SOD-Cys(6)H^+) is derived from a Cys(6)S/N^{amine}/N^{amide} (σ)−Ni($3d_{xz}+3d_{xy}$) antibonding interaction.

Upon the addition of the water molecule to the Cys(6) protonated model (Ni^{II}(SOD-Cys(6)H^+)$\cdots H_2O$), the LUMO and HOMO remain relatively unchanged compared with water-free Ni^{II}(SOD-Cys(6)H^+), save an increase in S-character to the LUMO. This increase in covalency to the LUMO is due to

dx.doi.org/10.1021/ja5079514 | J. Am. Chem. Soc. 2014, 136, 16009−16022

the contraction of the Cys(6) Ni−S bond upon protonation, which enhance S−Ni σ-bonding in the xy plane. We also note that there appears to be electronic communication through the S···H_2O hydrogen bonds as there is a small amount of electron density residing on the water O atom in the HOMO; the HOMO contains ∼1.2% water O($2p_{z/y}$) character. Other influences on the electronic structure are also induced upon water molecule hydrogen bonding. Owing to protonation and the hydrogen-bonding of water to Cys(6), the HOMO−1 becomes similar to the HOMO−1 of Ni^{II}(SOD-Cys(6)Me); it is best described as a Cys(2)S/N^{amide}(π)-Ni(3dπ) antibonding orbital. There is also a small contribution from the water O($2p_{z/y}$) atomic orbitals to the HOMO−1 (<1%). The HOMO−2 is no longer a Ni($3d_{z^2/xy}$)-S(σ) antibonding orbital, which is now the HOMO−3. Instead, the HOMO−2 is comprised of a highly covalent N/O(σ)+Ni(3dπ) bonding interaction with virtually no S character because the symmetry appropriate S(3pπ)-type AOs are utilized for H^+ and hydrogen bonding.

Sulfur K-edge Studies of {Ni^{II}(SOD^{m1}C(6)C^{Me})} and {Ni^{II}(SOD^{m1})}. Figure 3a displays the S K-edge X-ray absorption spectrum of {Ni^{II}(SOD^{m1}C(6)C^{Me})} and the pH 7.4 and 9.5

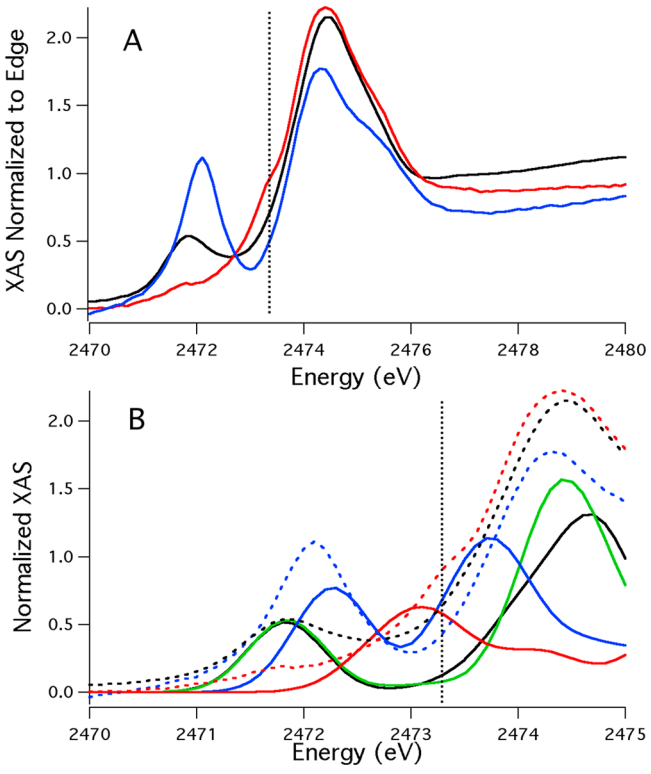

Figure 3. (A) Sulfur K-edge X-ray absorption spectrum of {Ni^{II}(SOD^{m1}C(6)C^{Me})} (black) and {Ni^{II}(SOD^{m1})} at pH 7.4 (red) and pH 9.5 (blue). The vertical black line indicates the edge position in the pH 7.4 {Ni^{II}(SOD^{m1})} spectrum corresponding to the unprotonated S(1s) → Ψ_1* transition. (B) TD-DFT calculated pre-edge regions of the S K-edge X-ray absorption spectra of (Ni^{II}(SOD))$^-$ (blue), Ni^{II}(SOD-Cys(6)Me) (black), Ni^{II}(SOD-Cys-(6)H^+) (green), and Ni^{II}(SOD-Cys(6)H^+)···H_2O (red). The experimental data for {Ni^{II}(SOD^{m1}C(6)C^{Me})} (dashed black) and {Ni^{II}(SOD^{m1})} at pH 7.4 (dashed red) and pH 9.5 (dashed blue) are included for comparison. The intensities of the transitions were normalized to the experimental pre-edge transition intensity of {Ni^{II}(SOD^{m1}C(6)C^{Me})}. The vertical black line indicates the edge feature position in the experimental pH 7.4 {Ni^{II}(SOD^{m1})} spectrum.

spectra of {Ni^{II}(SOD^{m1})}. For most transition-metal thiolate compounds with one or more holes in the nd-set the S K-edge X-ray absorption spectrum contains a pre-edge feature that is resolved from the edge. This peak corresponds to a S(1s) → Ψ_1* transition, where Ψ_1* is the lowest-energy acceptor state. For these metallopeptides Ψ_1* is predominately Ni($3d_{x^2-y^2}$) in character. As S K-edge XAS is an atomic spectroscopy the acceptor state must contain sulfur character. Therefore, the S(1s) → Ψ_1* transition gains intensity through the mixing of S(3p) character into the acceptor state. Thus, integration of the pre-edge feature provides a direct measurement of metal-thiolate covalency in such compounds. The integrated intensity of the S(1s) → Ψ_1* transition, $I_{S(1s)\rightarrow\Psi1*}$, can be related to the degree of S(3p) character in the acceptor state by

$$I_{S(1s)\rightarrow\Psi1*} = \alpha^2 I_{S(1s)\rightarrow S(3p)} \quad (2)$$

where α^2 is the S(3p) ligand coefficient of the acceptor orbital wave function and $I_{S(1s)\rightarrow S(3p)}$ is the intensity of a purely ligand centered transition.[25−27]

The S K-edge X-ray absorption spectrum for {Ni^{II}(SOD^{m1}C-(2)C^{Me})} displays a sharp transition at 2471.8(1) eV corresponding to the thiolate S(1s) → Ψ_1* transition. The thioether-based S(1s) → Ψ_1* transition occurs at higher energy and is buried in the edge. The integrated intensity for the thiolate S(1s) → Ψ_1* transition is 0.43(1) units, which correlates to a %S(3p) character of 16(4)% to Ψ_1*.[43]

The pH 9.5 S K-edge X-ray absorption spectrum for {Ni^{II}(SOD^{m1})} also displays a sharp pre-edge feature, which is slightly blue-shifted relative to the {Ni^{II}(SOD^{m1}C(6)C^{Me})} pre-edge peak (2472.1(1) eV). This reflects an overall destabilization of Ψ_1* in the high pH form of {Ni^{II}(SOD^{m1})} relative to {Ni^{II}(SOD^{m1}C(6)C^{Me})}. This is consistent with the above disclosed hybrid DFT studies; (Ni^{II}(SOD))$^-$ displays a destabilized LUMO relative to Ni^{II}(SOD-Cys(6)Me) owing to a more covalent Ni−S(σ) bonding interaction. The intensity of this transition is 0.98(2) units, which correlates to a %S(3p) character to Ψ_1* of 36(6)%.[40] Upon lowering the solution pH to 7.4 the pre-edge feature observed in the pH 9.5 S K-edge X-ray absorption spectrum of {Ni^{II}(SOD^{m1})} disappears and the edge broadens (Figure 3).

To better understand the physical origin of the differences in the above spectra, we simulated the S K-edge X-ray absorption spectra of (Ni^{II}(SOD))$^-$, Ni^{II}(SOD-Cys(6)Me), Ni^{II}(SOD-Cys(6)H^+), and Ni^{II}(SOD-Cys(6)H^+)···H_2O using TD-DFT methods at the PBE0/def2-tzvp(-f) level (Figure 3B).[41] The simulated spectra for both (Ni^{II}(SOD))$^-$ and Ni^{II}(SOD-Cys(6)Me) reproduce their respective experimental spectra well; both reproduce the experimental low-energy thiolate-based S(1s) → Ψ_1* transitions. Furthermore, the pre-edge feature calculated for (Ni^{II}(SOD))$^-$ displays both an increase in intensity and a 0.4 eV blue shift in the transition energy relative to that calculated for Ni^{II}(SOD-Cys(6)Me), as was observed experimentally. The increase in the intensity of the S(1s) → Ψ_1* transition observed in (Ni^{II}(SOD))$^-$ relative to Ni^{II}(SOD-Cys(6)Me) is due to the fact that the pre-edge feature contains transitions originating from both thiolate sulfur atoms. In the case of Ni^{II}(SOD-Cys(6)Me) only the transition originating from the thiolate sulfur atom is observed in the pre-edge feature; the thioether-based transition is ∼2 eV higher in energy. Furthermore, there is an increase in Ni−S covalency in (Ni^{II}(SOD))$^-$, which leads to an increase in the intensity of its S(1s) → Ψ_1* transition. The experimentally determined values

dx.doi.org/10.1021/ja5079514 | J. Am. Chem. Soc. 2014, 136, 16009−16022

for S(3p) character to Ψ_1* are consistent with the calculated S(3p) composition of the LUMO wave functions for both $(Ni^{II}(SOD))^-$ and Ni^{II}(SOD-Cys(6)Me) (PBE0/def2-tzvp; Table 2). The calculated thiolate %S(3p) composition to the LUMO of $(Ni^{II}(SOD))^-$ is 44.6%, which is ~3% higher than the $\{Ni^{II}(SOD^{m1})\}$ pH 9.5 experimental value for Ψ_1* when the error in the measurement is taken into account. This could be a result of errors associated with the computational method or incomplete deprotonation of $\{Ni^{II}(SOD^{m1})\}$ at pH 9.5. The %S(3p) composition to the LUMO of Ni^{II}(SOD-Cys(6)Me) yielded a better match to the experimentally determined S(3p) character to Ψ_1* for $\{Ni^{II}(SOD^{m1}C(6)C^{Me})\}$. The thiolate % S(3p) composition to the LUMO is 13.0% for Ni^{II}(SOD-Cys(6)Me), which is within experimental error.

The calculated S K-edge X-ray absorption spectrum for $Ni^{II}(SOD\text{-}Cys(6)H^+)$ does not correlate with the low pH S K-edge X-ray absorption spectrum observed for $\{Ni^{II}(SOD^{m1})\}$ but instead correlates best with that observed for $\{Ni^{II}(SOD^{m1}C(6)C^{Me})\}$. This is because protonation vs methylation of Cys(6) has similar influences on the electronic structure of these metallopeptides. Similar to Ni^{II}(SOD-Cys(6)Me), the unprotonated thiolate of $Ni^{II}(SOD\text{-}Cys(6)H^+)$ yields a low-energy S(1s) → Ψ_1* transition, while the transition originating from the protonated thiolate S(1s) orbital occurs ~2 eV higher in energy.

In order to reproduce the experimental low pH S K-edge X-ray absorption spectrum of $\{Ni^{II}(SOD^{m1})\}$ a water molecule must be included in the computational model within hydrogen-bonding distance to the Cys(2) and Cys(6) thiolate sulfur atoms $(Ni^{II}(SOD\text{-}Cys(6)H^+)\cdots H_2O)$. The inclusion of the water molecule shifts both the unprotonated and protonated thiolate-based S(1s) → Ψ_1* transitions. The protonated thiolate-based transition shifts 0.1 eV higher energy relative to the water free model. The unprotonated thiolate-based transition displays a larger shift in energy (+0.8 eV). In the experimental data, this feature is observed as a shoulder in the edge (Figure 4, vertical dashed line).

Electronic Absorption and CD Measurements of $\{Ni^{II}(SOD^{m1}C(6)C^{Me})\}$ and $\{Ni^{II}(SOD^{m1})\}$. The previously reported $\{Ni^{II}(SOD^{m1})\}$ optical spectra[18] contained a $\{Ni^{III}(SOD^{m1})\}$ contaminant resulting from the oxidation of $\{Ni^{II}(SOD^{m1})\}$ by O_2. Furthermore, the electronic absorption and CD spectra reported for $\{Ni^{II}(SOD^{m1})\}$ were only analyzed at pH 7.4. As the Cys(6) protonation state and active-site hydration change upon pH elevation, we reanalyzed the spectra of $\{Ni^{II}(SOD^{m1})\}$ at low and high pH to compare with the optical data obtained for $\{Ni^{II}(SOD^{m1}C(6)C^{Me})\}$.

The electronic absorption spectra obtained for $\{Ni^{II}(SOD^{m1})\}$ (pH 7.4 and pH 9.5) and $\{Ni^{II}(SOD^{m1}C(6)\text{-}C^{Me})\}$ (pH 7.4) are displayed in Figures 4 and 5, respectively. As can be seen the absorption spectra of $\{Ni^{II}(SOD^{m1})\}$ (both high and low pH) and $\{Ni^{II}(SOD^{m1}C(6)C^{Me})\}$ are similar to one another. All three spectra display ligand-field bands in the range of 16,000−25,000 cm^{-1} with charge-transfer bands appearing at higher energies. These spectra are in fact reminiscent of all known square-planar $Ni^{II}N_2S_2$ complexes.[12,33,34,40,42−45] We note that these ligand-field transitions all gain intensity through the mixing of ligand character into the ground- and excited-state wave functions and are thus more intense than what would be predicted for typical square-planar Ni^{II} complexes. The CD spectra for both $\{Ni^{II}(SOD^{m1}C(6)\text{-}C^{Me})\}$ and $\{Ni^{II}(SOD^{m1})\}$ obtained at low pH are similar to one another. In contrast, the CD spectrum obtained for

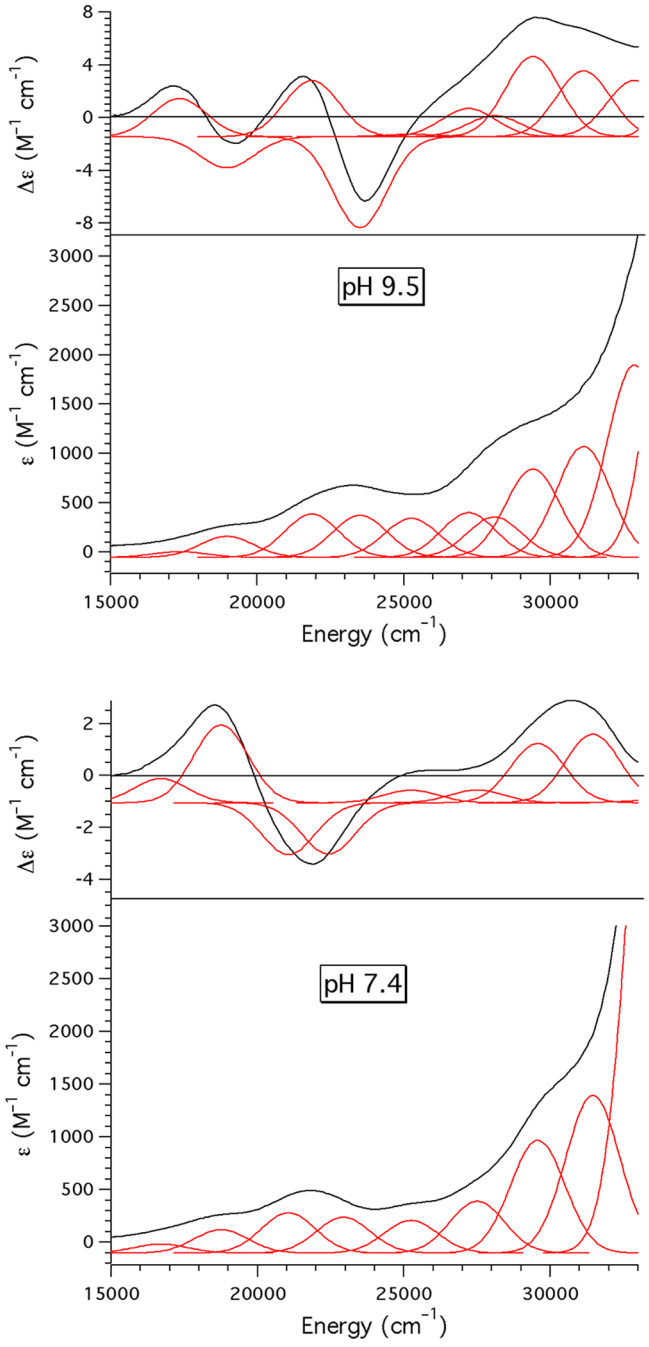

Figure 4. Electronic absorption and CD spectra of the pH 9.5 (top) and 7.4 (bottom) forms of $\{Ni^{II}(SOD^{m1})\}$. The individual deconvoluted transitions are given as the red Gaussian curves.

$\{Ni^{II}(SOD^{m1})\}$ at high pH is distinct from the other two in the low-energy region.

To understand the physical origin of these differences, simultaneous deconvolutions of the electronic absorption and CD spectra were performed by employing TD-DFT calculations (PBE0/def2-tzvp) on the computational models $Ni^{II}(SOD\text{-}Cys(6)Me)$, $Ni^{II}(SOD\text{-}Cys(6)H^+)\cdots H_2O$, and $(Ni^{II}(SOD))^-$. The calculated electronic absorption spectra match the experimental data further suggesting that these computational models are accurate geometric/electronic structural models for the metallopeptide-based systems (Supporting Information). We note that the TD-DFT spectrum obtained for $Ni^{II}(SOD\text{-}Cys(6)H^+)$ maps well onto

dx.doi.org/10.1021/ja5079514 | J. Am. Chem. Soc. 2014, 136, 16009−16022

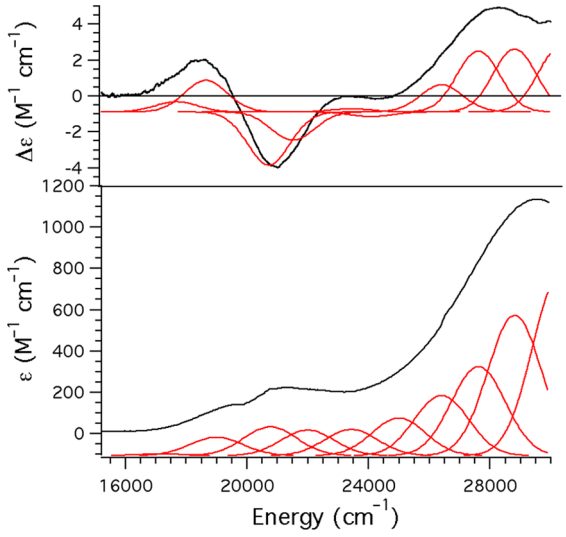

Figure 5. Electronic absorption and CD spectra of {NiII-(SODm1C(6)CMe)}. The individual deconvoluted transitions are given as the red Gaussian curves.

the theoretical spectrum obtained for Ni^{II}(SOD-Cys(6)Me) and not Ni^{II}(SOD-Cys(6)H^+)···H_2O nor $(Ni^{II}(SOD))^-$.

The assignments of the deconvolved bands can be found in the Supporting Information (Tables S20−S22). Herein, only the main contributors differentiating the three spectra will be discussed. As noted above, the high pH form of {$Ni^{II}(SOD^{m1})$} displays differences in the low-energy region of its CD spectrum relative to both the low pH form of {$Ni^{II}(SOD^{m1})$} and {$Ni^{II}(SOD^{m1}C(6)C^{Me})$}. This is due to the large splitting of the low-energy symmetry related quasi-degenerate states that are comprised of an admixture of the HOMO and HOMO−1. This does not occur in {$Ni^{II}(SOD^{m1}C(6)C^{Me})$} or in the pH 7.4 form of {$Ni^{II}(SOD^{m1})$} as there is a larger energy difference between these two states than is found in deprotonated water-free {$Ni^{II}(SOD^{m1})$}.

Differences also exist between the spectra obtained for {$Ni^{II}(SOD^{m1}C(6)C^{Me})$} and the pH 7.4 form of {$Ni^{II}(SOD^{m1})$}. One difference is the increase in oscillator strength of the transition in {$Ni^{II}(SOD^{m1})$} (pH 7.4) vs {$Ni^{II}(SOD^{m1}C(6)C^{Me})$} owing to an increase in covalency. Another notable difference are the energies of the band identified as the Cys(2)S(π)-Ni($3d_{xz}$) → Cys(6)S(π) inter-ligand charge transfer (ILCT) band in the two spectra. The ILCT band is ∼3500 cm^{-1} higher in energy for {$Ni^{II}(SOD^{m1})$} (pH 7.4) relative to {$Ni^{II}(SOD^{m1}(SOD^{m1}C(6)C^{Me})$}. This can be largely rationalized by the destabilization of the Cys(6)-based acceptor state upon Cys-S hydrogen-bonding to H_2O.

Computationally Derived Mechanism of the Superoxide Reduction Half-Reaction. To examine the influence of cysteinate protonation and the presence of a water molecule at the active-site of {$Ni^{II}(SOD^{m1})$} on the mechanism of O_2^- reduction, we computationally probed a potential superoxide reduction mechanism involving Ni^{II}(SOD-Cys(6)H^+) and Ni^{II}(SOD-Cys(6)H^+)···H_2O. Only an outersphere process was considered (see Discussion for more details). Potential energy surfaces (PESs) were constructed using a relaxed PES scan by transferring the Cys(6)S-H^+ proton to the O_2-molecule by systematically varying the H···O bond distance (BP86/def2-tzvp; COSMO). Multiple initial superoxide starting coordinates were investigated. The different starting positions consistently converged to a single PES for each structure. These PES scans yielded approximate hydrogen-bonded reactant, product, and TS structures, which were then refined (Figure 6). Single point/frequency calculations were then performed on these structures (PBE0/def2-tzvp). The resulting energies are corrected for solvation effects using a COSMO solvation model.

All attempts to derive an outersphere PES for superoxide reduction using the lowest-energy Ni^{II}(SOD-Cys(6)H^+)

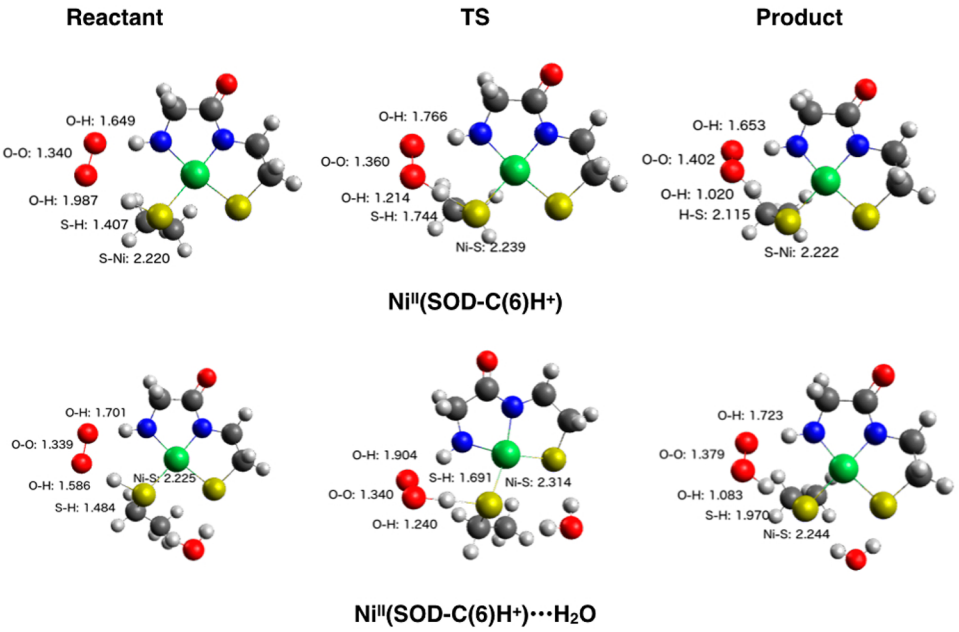

Figure 6. Reactant (left), TS (middle), and product (right) structures for superoxide reduction by Ni^{II}(SOD-Cys(6)H^+)* (top) and Ni^{II}(SOD-Cys(6)H^+)···H_2O (bottom; BP86/def2-tzvp). Relevant bond lengths are provided. The corresponding imaginary frequencies at the TS for Ni^{II}(SOD-Cys(6)H^+)* and Ni^{II}(SOD-Cys(6)H^+)···H_2O are −475 and −514 cm^{-1}, respectively (PBE0/def2-tzvp).

dx.doi.org/10.1021/ja5079514 | J. Am. Chem. Soc. 2014, 136, 16009−16022

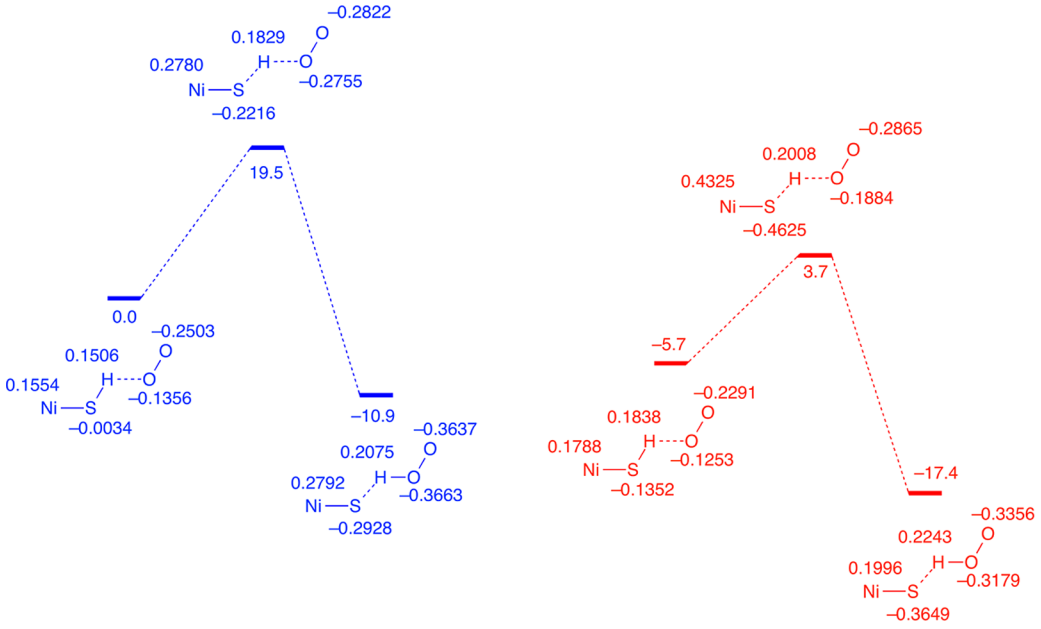

Figure 7. Free energy profile for the first step of the superoxide reduction reaction facilitated by Ni^{II}(SOD-Cys(6)H^+)···H_2O (right, red) and Ni^{II}(SOD-Cys(6)H^+)* (left, blue; PBE0/def2-tzvp). Free energies are given in kcal mol^{-1} and are all relative to the Ni^{II}(SOD-Cys(6)H^+)* reactant free energy. Mulliken atomic charges are given near the appropriate atoms.

structure failed; multiple trajectories of O_2^- approaching the Cys(6)-SH^+ moiety lead to either nonsensical geometries or a failure to adequately converge the wave functions using either different starting geometries and/or different SCF convergence strategies. We therefore altered the orientation of the Cys(6)-SH^+ moiety for the Ni^{II}(SOD-Cys(6)H^+) structure such that the Cys(6)S-H^+ proton was positioned within the H_2N^{amine}-Ni^{II}S-Cys(6) cleft generating Ni^{II}(SOD-Cys(6)H^+)* (Figure 6). Ni^{II}(SOD-Cys(6)H^+)* is 0.6 kcal mol^{-1} higher in free energy than Ni^{II}(SOD-Cys(6)H^+), suggesting that there is minimal interaction between the S−H^+ group and the Cys(2) sulfur atom. We note that rotation of the H^+ such that it is within the H_2N-Ni^{II}S-Cys(6) cleft allows for a hydrogen-bonding interaction between the approaching O_2^- molecule and the amine N-H moiety as well as the Cys(6)-SH^+ moiety. This both stabilizes the O_2^-··· Ni^{II}(SOD-Cys(6)H^+)* structures and effectively guides the O_2^- toward the active-site.

Reduction of superoxide proceeds as a concerted process with only one TS found for the transfer of both the proton and electron to superoxide. The overall free energy for the initial step of the superoxide reduction reaction is −10.9 kcal mol^{-1} with a transition state (TS) that lies at $\Delta G^{\ddagger}$ = 19.5 kcal mol^{-1} (Figure 7). The largest structural change upon going from reactant state to the TS is the movement of the Cys(6)S-H^+ proton toward an oxygen atom on the superoxide molecule. As would be expected, there is a lengthening of the O−O bond (from 1.34 to 1.36 Å at the TS) as the superoxide O−H bond contracts (from 1.99 to 1.21 Å at the TS). At the TS there is also a lengthening of the Ni−S bond *trans* to the amidate nitrogen. This is due to an increased buildup of S(3p) electron density on the Cys(6) sulfur center, which increases the repulsive filled/filled Ni(3dπ)−S(3π) interactions at the TS. Proceeding from the TS to the product state there is a further lengthening of the, now peroxide, O−O bond (1.40 Å) and a contraction of the Ni−S bond (2.22 Å).

At the TS the SOMO shows spin density distribution over the Ni−S electron donor orbitals and the O−O acceptor orbitals (Figure 8). Furthermore, the electron donor and acceptor orbitals are the same as the proton donor and acceptor

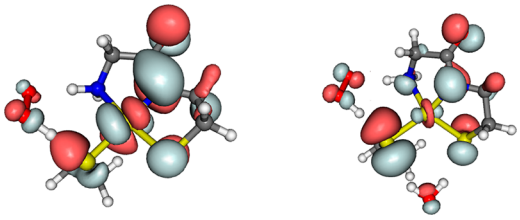

Figure 8. Isosurface plots of the SOMO for the HAT reaction between O_2^- and Ni^{II}(SOD-Cys(6)H^+)* (left) vs Ni^{II}(SOD-Cys(6)H^+)···H_2O (right).

orbitals. This may indicate that the reaction is a hydrogen atom transfer (HAT) reaction.[46]

The final model considered in a potential superoxide reduction mechanism was Ni(SOD-Cys(6)H^+)···H_2O, which contains the hydrogen-bonding interaction between a water molecule and the Cys(6) and Cys(2) sulfur atoms. This yields two desirable effects. First, the water-S hydrogen-bonding interaction naturally forces the transferring H^+ within the H_2N^{amine}-Ni^{II}S-Cys(6) cleft setting superoxide up for appropriate H atom attack as outlined above. The second effect is that it thermodynamically stabilizes Ni^{II}(SOD-Cys(6)H^+)··· H_2O relative to Ni^{II}(SOD-Cys(6)H^+) owing to the additional hydrogen-bonding interactions to the Cys sulfur atoms. This lowers the energy of the reactant state by ΔG = 5.7 kcal mol^{-1} relative to the model without the water molecule interaction. The resulting energetics on proceeding to the TS and product states are also lower than that calculated for Ni^{II}(SOD-Cys(6)H^+)* ($\Delta G^{\ddagger}$ = 8.4 kcal mol^{-1} and an overall ΔG = −11.7 kcal mol^{-1}).

There are other notable differences in the initial step of the O_2^- reduction reaction obtained for the two computational models. First, there is far less peroxide character at the TS for

dx.doi.org/10.1021/ja5079514 | J. Am. Chem. Soc. 2014, 136, 16009−16022

the reaction performed by $Ni^{II}(SOD\text{-}Cys(6)H^+)\cdots H_2O$ vs $Ni^{II}(SOD\text{-}Cys(6)H^+)$*. This is indicated by the fact that the O−O bond length remains virtually unchanged at the TS relative to the reactant state. There is also a longer O···H−N hydrogen bond and less negative charge build-up on the O_2^- molecule at the TS of the $Ni^{II}(SOD\text{-}Cys(6)H^+)\cdots H_2O$ facilitated reduction reaction than that of the $Ni^{II}(SOD\text{-}Cys(6)H^+)$* facilitated reduction reaction. Overall, this is suggestive of a TS that is more "PT-like" than that obtained for $Ni(SOD\text{-}Cys(6)H^+)$*. This is driven by the lowered calculated pK_a of the Ni(II)-$S(H^+)$-Cys in $Ni(SOD\text{-}Cys(6)H^+)\cdots H_2O$ (3.5) vs $Ni(SOD\text{-}Cys(6)H^+)$* (6.2) due to the water hydrogen bond to Cys(6).[38] Another difference is that at the TS the Cys(6) Ni−S bond of $Ni^{II}(SOD\text{-}Cys(6)H^+)\cdots H_2O$ is elongated relative to the Ni−S bond obtained for the TS-state structure of $Ni(SOD\text{-}Cys(6)H^+)$*. This is not a result of significant $Ni(3d\pi)/S(3p\pi)$ repulsion but instead is primarily attributed to a distortion of the Ni-center toward a more tetrahedral-like geometry. This distortion about the nickel center is likely necessitated to incorporate the water molecule at the active-site and still maintain appropriate orbital overlap for HAT.

Despite less peroxide character in the TS of the O_2^- reduction reaction facilitated by $Ni(SOD\text{-}Cys(6)H^+)\cdots H_2O$ vs $Ni(SOD\text{-}Cys(6)H^+)$, the SOMO at the TS for the $Ni(SOD\text{-}Cys(6)H^+)\cdots H_2O$ initiated reduction of O_2^- is qualitatively similar to that obtained for $Ni(SOD\text{-}Cys(6)H^+)$*. Formal H• transfer is facilitated through a Cys(6)-S(3p) type orbital to O_2^-. However, the electron density is more S-centered in the case of $Ni(SOD\text{-}Cys(6)H^+)\cdots H_2O$ than $Ni(SOD\text{-}Cys(6)H^+)$*, which is the result of the tetrahedral distortion observed at the TS. As the Ni center distorts there is a reduction in Ni−S covalency, which results in charge localization on the S atom. This increase in charge localization on the Cys(6)-S atom is stabilized by the hydrogen-bonding interaction between the sulfur atom and the water molecule, which also contributes $O(2p_z)$ character to the SOMO.

DISCUSSION

NiSOD maquettes derived from the NiSOD protein sequence have similar spectroscopic, reactive, and structural properties as the metalloenzyme.[12,16−24] A number of detailed studies have been performed using these maquettes to better understand the properties and mechanism of NiSOD itself. One major unresolved question is how closely related the NiSOD maquettes' reactivity and mechanism of catalysis are to NiSOD itself.[12]

A recent study by us demonstrated that a NiSOD maquette, $\{Ni^{II}(SOD^{m1}H(1)H^{Me})\}$, facilitated O_2^- reduction through a probable PCET mechanism.[16] This was based largely on kinetic (KIE ~20 at room temperature) and thermodynamic (pK_a and redox potential) arguments. Considering the similarities between $\{Ni^{II}(SOD^{m1}H(1)H^{Me})\}$ and other metallopeptides derived from the NiSOD sequence, such as $\{Ni^{II}(SOD^{m1})\}$, it was deemed a reasonable supposition that all of these metallopeptides facilitate O_2^- disproportionation through a similar mechanism. Therefore, the parent metallopeptide $\{Ni^{II}(SOD^{m1})\}$ was subjected to detailed studies to better define the details of its active-site. This information was then utilized to examine a viable mechanism for O_2^- reduction computationally, which can in-turn be used to make conclusions concerning the relationship between the superoxide disproportionation mechanism effected by $\{Ni^{II}(SOD^{m1})\}$ peptides vs NiSOD.

The pH 7.4 Active-Site Structure of $\{Ni^{II}(SOD^{m1})\}$. All of the available evidence points toward the formulation of the pH 7.4 active-site of $\{Ni^{II}(SOD^{m1})\}$ as presented in Chart 2.

Chart 2. Proposed Active-Site Structures of $\{Ni^{II}(SOD^{m1})\}$ at pH 7.4 and 9.5

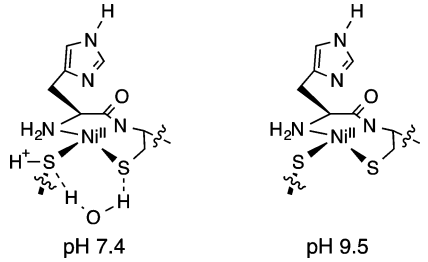

Several lines of evidence point toward the formulation of a protonated Ni^{II}-$S(H^+)$-Cys(6) moiety and at least one water contained within a Cys(2)/Cys(6) hydrogen bond at the $\{Ni^{II}(SOD^{m1})\}$ active-site. Of the *S*-methylcysteine-containing metallopeptides, only the Cys(6) *S*-methylated peptide is capable of coordinating Ni(II); both the Cys(2) and the Cys(2)/Cys(6) *S*-methylated peptide fail to ligate Ni(II) under any condition investigated. This suggests that protonation of the Cys(2) sulfur atom in $\{Ni^{II}(SOD^{m1})\}$ would release nickel from the peptide in aqueous solvent.

Examination of an array of computational models also suggests Cys(6) protonation and the association of one water molecule in a hydrogen-bonding network to Cys(2) and Cys(6). Consistent with the *S*-methylcysteine experimental results, computational studies suggest that Cys(6), not Cys(2), is the thermodynamically preferred protonation site. In addition, the geometric properties of the pH 7.4 form of $\{Ni^{II}(SOD^{m1})\}$ can only be reproduced using the Cys(6) protonated computational model. When Cys(6) is not protonated the average Ni−S bond length is longer than what is observed experimentally by >0.03 Å. An indication of Cys(2)/Cys(6) water association is the contraction of the average Ni−S bond lengths in the calculated model $Ni^{II}(SOD\text{-}Cys(6)H^+)\cdots H_2O$ such that it matches the pH 7.4 EXAFS derived Ni−S bond lengths for $\{Ni^{II}(SOD^{m1})\}$. A similar influence on Ni−S bond lengths upon their interaction with hydrogen-bond donors was observed by Harrop in a small molecule NiSOD mimic.[34] We note that the difference in the average calculated bond lengths for $Ni^{II}(SOD\text{-}Cys(6)H^+)$ and $Ni^{II}(SOD\text{-}Cys(6)H^+)\cdots H_2O$ is 0.014 Å, which could relate to inadequacies in the computational methods used coupled with the error in the EXAFS derived bond lengths of $\{Ni^{II}(SOD^{m1})\}$. However, S K-edge spectroscopy strongly suggests that there is indeed a water molecule associated with the active-site of $\{Ni^{II}(SOD^{m1})\}$ at pH 7.4.

The S K-edge spectroscopic data for the high pH form of $\{Ni^{II}(SOD^{m1})\}$ can be readily rationalized in terms of the structure outlined in Chart 2 (no Cys protonation and no water hydrogen bonding to the active-site). The S K-edge spectrum yields the expected thiolate S(1s) → Ψ_1* transition with covalency parameters that correlate well with the computationally expected values. The electronic absorption and CD spectra of $\{Ni^{II}(SOD^{m1})\}$ obtained at high pH are also fully consistent with the active-site formulation presented in Chart 2. Similarly, $\{Ni^{II}(SOD^{m1}C(6)C^{Me})\}$ yields fully consistent S K-edge and

dx.doi.org/10.1021/ja5079514 | J. Am. Chem. Soc. 2014, 136, 16009−16022

optical spectra with an active-site formulation of a methylated Cys(6) sulfur atom and no water association at the active-site.

Computational studies demonstrate that Cys(6) protonation vs methylation of $\{Ni^{II}(SOD^{m1})\}$ yield virtually identical electronic structures and spectroscopic signatures demonstrating that $\{Ni^{II}(SOD^{m1}C(6)C^{Me})\}$ can be used as a mimic of Cys(6) protonated $\{Ni^{II}(SOD^{m1})\}$. However, $\{Ni^{II}(SOD^{m1}C(6)C^{Me})\}$ is spectroscopically and structurally distinct from $\{Ni^{II}(SOD^{m1})\}$ under low pH conditions, suggesting that simple protonation of Cys(6) alone cannot be used to rationalize the available data. It is only upon the addition of a water molecule contained in a hydrogen-bonding network to Cys(2) and Cys(6) that the S K-edge XAS and optical spectra can be fully rationalized. The lack of a well-resolved thiolate S(1s) → Ψ_1* transition can be rationalized by the proposal hydrogen bonding to the Cys(2) thiolate effectively blue-shifts the transition into the edge. In fact, this thiolate S(1s) → Ψ_1* transition is observed as a shoulder feature in the edge of the experimental low pH S K-edge spectrum of $\{Ni^{II}(SOD^{m1})\}$.

In a study examining water hydrogen bonding to Ni and Fe thiolates, Solomon and co-workers found that the S K-edge XAS pre-edge transition of a bis-amine $Ni^{II}N_2S_2$ complex (Ni(DACO)) shifted by +0.2 eV upon water hydrogen bonding in dry acetonitrile.[47] Water association in the Ni^{II}(SOD-Cys(6)H^+)···H_2O computational model yields a Ni−S bond contraction relative to $(Ni^{II}(SOD))^-$ and an increase in the S(3p) contribution to the LUMO, neither of which are seen in Ni(DACO) upon water hydrogen bonding. Thus, a larger shift of the thiolate S(1s) → Ψ_1* transition energy is produced in Ni^{II}(SOD-Cys(6)H^+)···H_2O than observed in Ni(DACO).

All of the spectroscopic data for the low pH form of $\{Ni^{II}(SOD^{m1})\}$ can be rationalized using a computational model containing only one water molecule associated with the cysteinate sulfur atoms within the primary hydration sphere. It was deemed possible that additional important water−active site interactions are present in the low pH form of $\{Ni^{II}(SOD^{m1})\}$. When an additional water molecule is placed about the thiolate S atoms in the Ni^{II}(SOD-Cys(6)H^+)···H_2O computational model, it does not associate directly with the primary coordination sphere (Supporting Information). Instead, the additional water molecule hydrogen bonds to the associated water molecule (i.e., it would be associated with the hydration sphere). This imparts no significant change to the electronic or geometric structure of the nickel center. Thus, the active-site structures presented in Chart 2 likely represent the important interactions that contribute to the properties of $\{Ni^{II}(SOD^{m1})\}$.

The differences in active-site water association between the active-sites probed (i.e., $\{Ni^{II}(SOD^{m1}C(6)C^{Me})\}$ vs the high and low pH forms of $\{Ni^{II}(SOD^{m1})\}$) may be due to differences in the peptide environment about the Ni center in the metallopeptides. Owing to the likely Cys(6) methyl group orientation, $\{Ni^{II}(SOD^{m1}C(6)C^{Me})\}$ possesses a more hydrophobic S−Ni^{II}−S cleft where water would hydrogen bond to the cysteinates. The methyl group also yields steric crowding about the already congested water hydrogen-bonding site as well. Both of these may prevent water association to Cys(2) and Cys(6). Changes in peptide conformation at high vs low pH may also prevent water from associating at the active-site of the high pH form of $\{Ni^{II}(SOD^{m1})\}$ due to steric crowding.

Mechanistic Insight Into the Superoxide Reduction Half Reaction Facilitated by $\{Ni^{II}(SOD^{m1})\}$. In this study we computationally probed an outersphere mechanism for the $\{Ni^{II}(SOD^{m1})\}$ catalyzed reduction of O_2^-. The first step of the superoxide reduction mechanisms for both water-free Cys(6) protonated Ni^{II}(SOD-Cys(6)H^+) and water associated Ni^{II}(SOD-Cys(6)H^+)···H_2O was considered. We deemed an outersphere process for the reduction of O_2^- by $\{Ni^{II}(SOD^{m1})\}$ most likely based on the fact that, with the exception of stoichiometric amounts of cyanide, no exogenous ligands have been shown to be capable of binding to the Ni^{II} center of NiSOD,[39] $\{Ni^{II}(SOD^{m1})\}$,[48] other NiSOD maquettes[19] or the vast majority of amidate-containing $Ni^{II}N_2S_2$ complexes with one notable exception (*vide infra*).[44,49] These exogenous ligands include halides and superoxide-like mimics such as N_3^- and NO•. In addition to electronic factors, we suspect that exogenous ligands may be incapable of binding to the nickel center of NiSOD maquettes for steric reasons. $\{Ni^{II}(SOD^{m1})\}$, and other similar maquettes, lacks the outersphere hydrogen bonds found in NiSOD that may be important in maintaining an open loop-like structure that would allow superoxide to access the nickel center. DFT geometry optimizations performed on a peptide-based computational model comprised of the first six residues of the NiSOD N-terminus shows that the peptide-loop and histidine imidazole group effectively block O_2^- from accessing the Ni^{II} center (Figure 9). In contrast to the sterically restricted Ni^{II} center of $\{Ni^{II}(SOD^{m1})\}$, the H_2N−Ni(II)-Cys(6)H^+ cleft is well exposed to solvent making it accessible for O_2^- attack (Figure 9). This is the location where we propose O_2^- abstracts a formal H• from the $\{Ni^{II}(SOD^{m1})\}$ active site.

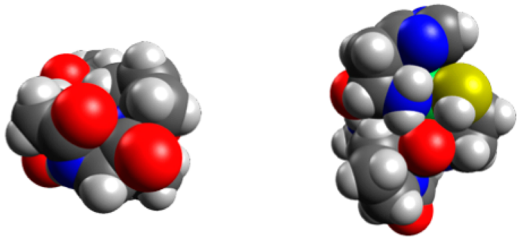

Figure 9. Space filling models of two different orientations of the geometry optimized structure (BP86/def2-tzvp) for the peptide-loop structure of $\{Ni^{II}(SOD^{m1})\}$ looking down the loop (right) and at the Ni(II)-S(H^+)-H_2N cleft (left).

A similarly crowded nickel center was formulated using NMR spectroscopic studies performed by Tietze and co-workers on an 8-mer NiSOD maquette.[24] In that study a CN^- anion was proposed to be associated within the active-site, bound directly to Ni in a highly unusual η^2 fashion as opposed to the typically observed end-on fashion through the cyanide C atom. If correct, this binding mode is likely necessitated by the steric crowding imposed by the peptide loop folding over the nickel center. The CN^- ligand is thus prevented from coordinating to Ni^{II} in the more typical linear end-on fashion. We also note that Tietze's study indicated that a cysteinate S-hydrogen-bonded water molecule was likely present at the nickel active-site, further supporting our active-site formulation for $\{Ni^{II}(SOD^{m1})\}$.

The computational investigations disclosed above seem to suggest a reaction mechanism that may be described as a HAT-like reaction. Although these studies suggest that a HAT-like reaction can occur from the site lacking the Cys(2)/Cys(6)··· water hydrogen-bonding interaction (i.e., Ni(SOD-Cys(6))*), it is not as facile as when this interaction is present; the

dx.doi.org/10.1021/ja5079514 | J. Am. Chem. Soc. 2014, 136, 16009−16022

activation barrier for H• transfer is over 10 kcal mol^{-1} higher in Ni^{II}(SOD-Cys(6)H^+)* vs Ni^{II}(SOD-Cys(6)H^+)···H_2O. Decomposition of the thermodynamic properties related to concerted proton- and electron-transfer (PT−ET) reactions (i.e., pK_a and Ni^{II}/Ni^{III} E_{ox}) suggests that the lowered reaction barrier in Ni^{II}(SOD-Cys(6)H^+)* vs Ni^{II}(SOD-Cys(6)H^+)···H_2O results from the increased acidity of the Cys-S(H^+)-Ni^{II} proton upon water hydrogen bonding to Cys(6). In contrast to the redox potentials, which remain virtually unaltered,[50] the Cys-S(H^+)-Ni^{II} proton in Ni^{II}(SOD-Cys(6)H^+)···H_2O has a pK_a three pK_a units lower than Ni^{II}(SOD-Cys(6)H^+). From a simple application of Marcus−Hush theory the higher acidity of the Ni^{II}(SOD-Cys(6)H^+)···H_2O proton relative to the Ni^{II}(SOD-Cys(6)H^+)* proton will destabilize the Ni^{II}(SOD-Cys(6)H^+)···H_2O reactant state, which will in turn reduce the minimum crossing point energy between the reactant and product PESs, thus resulting in a lowered activation barrier.

This computationally proposed mechanism is consistent with a mechanistic study published by us probing the O_2^- disproportionation kinetics/thermodynamics facilitated by {Ni^{II}(SOD^{m1}H(1)H^{Me})}.[16] First, the thermodynamic parameter obtained experimentally suggested that {Ni^{II}(SOD^{m1}H(1)-H^{Me})} is poised to reduce O_2^- through a PCET reaction. Equilibrium experiments between {$Ni^{II/III}$(SOD^{m1}H(1)H^{Me})} and TEMPO•/TEMPO-H placed the bond dissociation free energy (BDFE) for the abstractable H• within {Ni^{II}(SOD^{m1}H-(1)H^{Me})} at 75 kcal mol^{-1}. Application of a modified Bordwell equation[51] to the experimentally derived pK_a and E_{ox} values for {Ni^{II}(SOD^{m1}H(1)H^{Me})} (pK_a ∼ 8.4; E_{ox} ∼ 0.44 V vs SHE) yielded a Ni^{II}-S(H^+)Cys BDFE of 79 kcal mol^{-1}. Both are less than the peroxide HO_2^- BDFE (81 kcal mol^{-1}),[51] thus {Ni^{II}(SOD^{m1}H(1)H^{Me})} is poised to reduce O_2^- to HO_2^- despite the fact that {Ni^{II}(SOD^{m1}H(1)H^{Me})} is neither thermodynamically capable of protonating (HO_2 pK_a = 4.69)[1] nor reducing superoxide (high pH O_2^- E_{red} = +0.20 V)[1] independent of the other process. We note that the computationally derived pK_a, $E_{1/2}$, and Ni^{II}-S(H^+)Cys BDFEs for Ni^{II}(SOD-Cys(6)H^+)* (80.1 kcal mol^{-1}) and Ni^{II}(SOD-Cys(6)H^+)···H_2O (75.6 kcal mol^{-1}) are in line with the experimentally derived values reported for {Ni^{II}(SOD^{m1}H(1)-H^{Me})}.

The other computationally derived thermodynamic properties for the O_2^- reduction reaction are also in line with the experimental data. On the basis of the {Ni^{II}(SOD^{m1}H(1)H^{Me})} H• BDFE it was speculated that the ΔG for the {Ni^{II}(SOD^{m1}H(1)H^{Me})} facilitated O_2^- reduction reaction is between −3 and −10 kcal mol^{-1}. The computationally derived Gibbs free energies for O_2^- reduction facilitated by Ni^{II}(SOD-Cys(6)H^+)* (ΔG = −10.9 kcal mol^{-1}) and Ni^{II}(SOD-Cys(6)H^+)···H_2O (ΔG = −11.7 kcal mol^{-1}) are therefore consistent with the experimentally derived ΔG for O_2^- reduction by these nickel centers.

The computationally derived observation that O_2^- reduction may proceed through a HAT process is also consistent with the kinetic data obtained for O_2^- reduction facilitated by {Ni^{II}(SOD^{m1}H(1)H^{Me})}. Superoxide disproportionation catalyzed by {Ni^{II}(SOD^{m1}H(1)H^{Me})} proceeds with a large room temperature solvent H/D KIE of ∼20. This strongly suggested: (a) H• movement in the rate limiting step and (b) a quantum mechanical tunneling component in the reaction mechanism. Our computational results support the notion of H• movement in the rate-limiting step of the superoxide reduction half-reaction facilitated by the {Ni(SOD^{m1})} family.

The proposed mechanism is based solely on an examination of the orbitals involved in ET and PT along the doublet PES.[32] It has been noted that it is difficult to distinguish between HAT vs PCET vs consecutive PT/ET reactions on the basis of MO arguments alone.[52,53] The fact that minimal charge transfer to superoxide is observed at the TS for the O_2^- reduction reaction facilitated by Ni^{II}(SOD-Cys(6)H^+)···H_2O may indicate that the PT−ET mechanism is not as simple as outlined above. Therefore, a study probing the more detailed aspects of the proposed reaction mechanism, such as adiabaticity and quantum mechanical tunneling, is forthcoming.

Biological Relevance of {Ni^{II}(SOD^{m1})} to NiSOD. Considering the similarities in the spectroscopic and structural data between these NiSOD maquettes and NiSOD itself, it is probable that NiSOD possesses a Ni^{II}-S(H^+)-Cys(6) moiety and additional hydrogen bonds to the coordinated cysteinate sulfur atoms. Alternatively, multiple hydrogen bonds to Cys(6) and a Ni^{II}-S(H^+)-Cys(2) moiety might also be envisioned. These hydrogen bonds and the protonated Ni^{II}-cysteinate are likely responsible for the observed spectroscopic and geometric properties of reduced NiSOD, which cannot be adequately reproduced in their absence.

Functionally, these hydrogen bonds and cysteinate protonation likely serve two purposes. One is to fine-tune the physical properties of the nickel center for optimal SOD catalysis. Another likely role is protection of the cysteinate sulfurs from oxidative damage induced by O_2 and H_2O_2. We, and others, have commented on the robustness of the NiSOD active site toward ROSs.[12,21,34,40,42,54−56] The Grapperhaus research group and our research group have suggested this is due (in part) to the electronic consequences of the mixed amine/amidate ligand set.[21,40,42,54] Harrop and Grapperhaus have also suggested that hydrogen bonds to the cysteinate sulfurs will protect the cysteinates from oxidative damage induced by ROSs.[34,54] This study shows that {Ni^{II}(SOD^{m1})} contains both a Ni^{II}-S(H^+)-Cys(6) moiety and water cysteinate hydrogen bonds, which likely enhance its observed robustness against oxidative damage in addition to the electronic fine-tuning of the Ni−S bond imparted by the primary coordination environment. A similar protective mechanism is likely occurring in NiSOD itself.

Concerning the proposed mechanism for O_2^- reduction by {Ni^{II}(SOD^{m1})}, there are several lines of evidence pointing to the fact that the proposed mechanism is *not* valid for NiSOD itself. The first comes from the observation that the kinetics of NiSOD catalysis is virtually pH independent.[37,57] This shows that proton movement is not rate-limiting in the enzymatic process and strongly argues against a concerted ET-PT process.

A second line of evidence that the above mechanism is not biologically valid comes from the NiSOD structure itself.[13−15] An approach of the O_2^- molecule toward the proton in the H_2N−Ni(II)-Cys(6)H^+ cleft as proposed for {Ni^{II}(SOD^{m1})} is impossible to achieve in the metalloenzyme. Instead, the only access point of superoxide to the nickel center involves O_2^- traveling down a protein channel ending in the open nickel-binding loop structure. Outersphere ET from the Ni(II) center of NiSOD to O_2^- as superoxide approaches the active-site could then occur.

It is also possible that an inner-sphere mechanism is occurring in the metalloenzyme itself. Such an innersphere process was considered by Pelmenschikov and Siegbahn in a hybrid DFT study probing the NiSOD mechanism.[58] In that study an innersphere mechanism was demonstrated to be

feasible. In addition to an inner- vs outersphere process, Pelmenschikov's mechanism was distinct from ours in that (a) the Ni^{II} center was considered to be in the $S = 1$, not $S = 0$ spin-state; (b) the mechanism is best described as an ET process followed by a PT process; and (c) Cys(2), not Cys(6), was considered as the proton donor. The proposal that Cys(2) is the likely proton donor is because the Cys(6) sulfur atom will not effectively position the H^+ toward the active-site and therefore makes for a less effective PT process to the coordinated O_2^{2-} than that facilitated by Cys(2).

A recent study by Masuda and co-workers lends further support to a possible innersphere superoxide disproportionation mechanism.[44] In their study a small molecule mixed amine/amidate square-planar NiN_2S_2 complex facilitated superoxide reduction and oxidation. In the absence of protons or an axial ligand the coordinated superoxide behaves as a pseduohalide. Reduction of superoxide within the purported $Ni^{II}-O_2^-$ adduct was only effected by the addition of both protons and an axial imidazole ligand to the nickel center. Such a mechanism is unlikely to occur in $\{Ni^{II}(SOD^{m1})\}$. Owing to steric constraints O_2^- can only coordinate to $\{Ni^{II}(SOD^{m1})\}$ in the same position where the axial histidine imidazole would coordinate. Additional axial ligation to the vacant site of the five coordinate superoxide adduct would be precluded for steric reasons. Because superoxide reduction appears to necessitate the formation of a six-coordinate Ni^{II} species, O_2^- reduction would not occur. We also note that unlike Pelmenschikov and Siegbahn's mechanism, the proton source proposed by Masuda was the coordinated amine N−H group, negating the need for the direct involvement of the Ni(II)-S(H^+)-Cys group in catalysis. If true the positioning of the Ni(II)-S(H^+)-Cys proton toward the active-site may be irrelevant for catalysis negating the need for Cys(2) protonation in the mechanism.

In summary, NiSOD maquettes derived from the primary NiSOD sequence remain useful mimics for understanding the electronic and geometric structure of NiSOD. However, considering the above observations, any disproportionation mechanism operable in NiSOD itself would have very little relationship to the O_2^- disproportionation mechanism of these maquettes. Thus, direct insight into the enzymatic disproportionation mechanism gained from such mimics may be tenuous at best.

■ ASSOCIATED CONTENT

Supporting Information

Contains experimental details, Cartesian coordinates for all computational models discussed, calculated electronic absorption spectra, $SOD^{m1}C(6)C^{Me}$ glycine competitive Ni(II) binding assay results, and spectroscopic parameters obtained from the Gaussian deconvolution of the experimental CD and electronic absorption spectra of $\{Ni^{II}(SOD^{m1})\}$ (pH 7.4 and 9.5) and $\{Ni^{II}(SOD^{m1})\}$. This material is available free of charge via the Internet at http://pubs.acs.org.

■ AUTHOR INFORMATION

Corresponding Author

shearer@unr.edu

Notes

The authors declare no competing financial interest.

■ ACKNOWLEDGMENTS

This work was supported by the National Science Foundation (CHE-1362662). All X-ray absorption studies were performed at the NSLS. Use of the National Synchrotron Light Source, Brookhaven National Laboratory, was supported by the U.S. Department of Energy, Office of Science, Office of Basic Energy Sciences, under contract no. DE-AC02-98CH10886. Ni K-edge studies were preformed on beamline X3-b, which is supported through the Case Center for Synchrotron Biosciences, which is funded through the National Institute of Biomedical Imaging and Bioengineering (NIH grant no. P30-EB-009998)

■ REFERENCES

(1) Sawyer, D. T.; Valentine, J. S. *Acc. Chem. Res.* **1981**, *14*, 393−400.
(2) Valentine, J. S.; Wertz, D. L.; Lyons, T. J.; Liou, L. L.; Goto, J. J.; Garalla, E. B. *Curr. Opin. Chem. Biol.* **1998**, *2*, 253−262.
(3) Miller, A.-F. *Curr. Opin. Chem. Biol.* **2004**, *8*, 162−168.
(4) Broering, E. P.; Truong, P. T.; Gale, E. M.; Harrop, T. C. *Biochemistry* **2013**, *52*, 4−18.
(5) Bryngelson, P. A.; Maroney, M. J. *Nickel Superoxide Dismutase. In Metal Ions in Life Sciences*; Sigel, A., Sigel, H., Sigel, R. K. O., Eds.; John Wiley & Sons, Ltd.: England, 2007; Vol. *2*, pp 417−444.
(6) Fridovich, I. In *Encyclopedia of Biological Chemistry*, 1st ed.; Lennarz, W. J., Lane, M. D., Eds.; Elsevier: New York, 2004; Vol. *4*, pp 135− 138.
(7) Kurtz, D. M., Jr. *Acc. Chem. Res.* **2004**, *37*, 902−908.
(8) Youn, H.-D.; Kim, E.-J.; Roe, J.-H.; Hah, Y.-C.; Kang, S.-O. *Biochem. J.* **1996**, *318*, 889−896.
(9) Youn, H.-D.; Youn, H.; Lee, J.-W.; Hah, Y.-C.; Kang, S.-O. *Arch. Biochem. Biophys.* **1996**, *334*, 341−348.
(10) Palenik, B.; Brahamsha, B.; Larimer, F. W.; Land, M.; Hauser, L.; Chain, P.; Lamerdin, J.; Regala, W.; A llen, E. E.; McCarren, J.; Paulsen, I.; Dufresne, A.; Partensky, F.; Webb, E. A.; Waterbury, J. *Nature* **2003**, *424*, 1037−1042.
(11) DuPont, C. L.; Neupane, K.; Shearer, J.; Palenik, B. *Environ. Microbiol.* **2008**, *10*, 1831−1843.
(12) Shearer, J. *Acc. Chem. Res.* **2014**, *47*, 2332−2341.
(13) Wuerges, J.; Lee, J.-W.; Yim, Y.-I.; Yim, H.-S.; Kang, S.-O.; Carugo, K. D. *Proc. Natl. Acad. Sci. U. S. A.* **2004**, *101*, 8569−8574.
(14) Barondeau, D. P.; Kassmann, C. J.; Bruns, C. K.; Tainer, J. A.; Getzoff, E. D. *Biochemistry* **2004**, *43*, 8038−8047.
(15) Herbst, R. W.; Guce, A.; Bryngelson, P. A.; Higgins, K. A.; Ryan, K. C.; Cabelli, D. E.; Garman, S. C.; Maroney, M. J. *Biochemistry* **2009**, *48*, 3354−3369.
(16) Shearer, J. *Angew. Chem., Int. Ed.* **2013**, *52*, 2569−2572.
(17) Shearer, J.; Long, L. M. *Inorg. Chem.* **2006**, *45*, 2358−2360.
(18) Neupane, K. P.; Shearer, J. *Inorg. Chem.* **2006**, *45*, 10552−10566.
(19) Neupane, K. P.; Gearty, K.; Francis, A.; Shearer, J. *J. Am. Chem. Soc.* **2007**, *129*, 14605−14618.
(20) Shearer, J.; Neupane, K. P.; Callan, P. E. *Inorg. Chem.* **2009**, *48*, 10560−10571.
(21) Shearer, J. *J. Inorg. Biochemistry* **2013**, *129*, 145−149.
(22) Schmidt, M.; Zahn, S.; Carella, M.; Ohlenschlager, O.; Gorlach, M.; Kothe, E.; Weston, J. *ChemBioChem* **2008**, *9*, 2135−2146.
(23) Tietze, D.; Breitzke, H.; Imhof, D.; Kothe, E.; Weston, J.; Buntkowsky, G. *Chem.−Eur. J.* **2004**, *15*, 5517−523.
(24) Tietze, D.; Voigt, S.; Mollenhauer, D.; Tischler, M.; Imhof, D.; Gutmann, T.; Gonzalez, L.; Ohlenschlager, O.; Breitzke, H.; Gorlach, M.; Buntkowsky, G. *Angew. Chem., Int. Ed.* **2011**, *50*, 2946−2950.
(25) Glaser, T.; Hedman, B.; Hodgson, K. O.; Solomon, E. I. *Acc. Chem. Res.* **2000**, *33*, 859−868.
(26) Neese, F.; Hedman, B.; Hodgson, K. O.; Solomon, E. I. *Inorg. Chem.* **1999**, *38*, 4854−4860.
(27) Solomon, E. I.; Hedman, B.; Hodgson, K. O.; Dey, A.; Szilagyi, R. K. *Coord. Chem. Rev.* **2005**, *249*, 97−129.

(28) Szilagyi, R. K.; Bryngelson, P. A.; Maroney, M. J.; Hedman, B.; Hodgson, K. O.; Solomon, E. I. *J. Am. Chem. Soc.* **2004**, *126*, 3018−3019.
(29) Colpas, G. J.; Maroney, M. J.; Bagyinka, C.; Kumar, M.; willis, W. S.; Suib, S. L.; Mascharack, P. K.; Baidya, N. *Inorg. Chem.* **1991**, *30*, 920−928.
(30) The EXAFS data can be modeled such that the Ni-−S shell is divided into two scatterers with one Ni−S scatterer at 2.17 Å and one at 2.21 Å (Supporting Information). However, these shells are to close for them to be resolved based on the quality of the data presented ($\Delta r = \pi/(2\Delta k)$ with Δk = 13 $Å^{-1}$).
(31) In these computational models Cys(6) will refer to the thiolate sulfur atom *trans* to the amidate nitrogen atom, and Cys(2) will refer to the thiolate sulfur atom *trans* to the amine nitrogen atom for ease of reference to the NiSOD and {$Ni^{II}(SOD^{m1})$} active-site.
(32) NEVPT2 calculations using a CAS(3,6) active space suggest that there is minimal multiconfigurational character to the ground-state wave function suggesting single determinant methods are sufficient to describe these systems.
(33) Gale, E. W.; Patra, A. K.; Harrop, T. C. *Inorg. Chem.* **2009**, *48*, 5620−5622.
(34) Gale, E. M.; Narendrapurapu, B. S.; Simmonett, A. C.; Schaefer, H. F., III; Harrop, T. C. *Inorg. Chem.* **2010**, *49*, 7080−7096.
(35) Grapperhaus, C. A.; Darensbourg, M. Y. *Acc. Chem. Res.* **1998**, *31*, 451−459.
(36) Farmer, P. J.; Reibenspies, J. H.; Lindahl, P. A.; Darensbourg, M. Y. *J. Am. Chem. Soc.* **1993**, *115*, 4665.
(37) Choudhury, S. B.; Lee, J.-W.; Davidson, G.; Yim, Y.-I.; Bose, K.; Sharma, M. L.; Kang, S.-O.; Cabelli, D. E.; Maroney, M. J. *Biochemistry* **1999**, *38*, 3744−3752.
(38) There is a potential error associated with these values as they are derived from a mixture of computational (at the PBE0/def2-tzvp level) and experimental values; see Supporting Information for full details.
(39) Fiedler, A. T.; Bryngelson, P. A.; Maroney, M. J.; Brunold, T. C. *J. Am. Chem. Soc.* **2005**, *127*, 5449−5462.
(40) Shearer, J.; Dehestani, A.; Abanda, F. *Inorg. Chem.* **2008**, *47*, 2649−2660.
(41) DeBeer George, S.; Neese, F. *Inorg. Chem.* **2010**, *49*, 1849−1853.
(42) Shearer, J.; Zhao, N. *Inorg. Chem.* **2013**, *45*, 9637−9639.
(43) Mathrubootham, V.; Thomas, J.; Staples, R.; McCraken, J.; Shearer, J.; Hegg, E. L. *Inorg. Chem.* **2010**, *49*, 5393−5406.
(44) Nakane, D.; Wasada-Tsutsui, Y.; Funahashi, Y.; Hatanaka, T.; Ozawa, T.; Masuda, H. *Inorg. Chem.* **2014**, *53*, 6512−6523.
(45) Kruger, H. J.; Peng, G.; Holm, R. H. *Inorg. Chem.* **1991**, *30*, 734−742.
(46) Mayer, J. M.; Hrovat, D. A.; Thomas, J. L.; Borden, W. T. *J. Am. Chem. Soc.* **2002**, *124*, 11142−11147.
(47) Dey, A.; Green, K. N.; Jenkins, R. M.; Jeffrey, S. P.; Darensbourg, M.; Hodgson, K. O.; Hedman, B.; Solomon, E. I. *Inorg. Chem.* **2007**, *46*, 9655−9660.
(48) In this study we have probed the ability of {$Ni^{II}(SOD^{m1})$} to coordinate N_3^-, Cl^-, Br^-, I^-, CN^-, and NO•. As reported with a similar metallopeptide (ref 19) the addition of over 3000 equiv of N_3^-, I^-, Br^-, and Cl^- yields no change in the electronic absorption spectrum of {$Ni^{II}(SOD^{m1})$}. The addition of CN^- removes Ni^{II} from the metallopeptide following the addition of greater than 2 equiv of cyanide. NO• addition results in metallopeptide decomposition likely owing to S-nitrosylation.
(49) We note a possible exception was recently reported where a mixed amine/amidate $Ni^{II}N_2S_2$ system was purported to coordinate superoxide; see ref 44. To our knowledge this is the only example of exogenous ligand coordination to a square-planar mixed amine/amidate $Ni^{II}N_2S_2$ complex.
(50) The redox potentials and S-H^+ pK_a vaules for Ni^{II}(SOD-Cys(6)H^+) (0.610 V vs SHE; pK_a = 6.2) vs Ni^{II}(SOD-Cys(6)H^+)···H_2O (0.571 V vs SHE; pK_a = 3.5) were calculated at the PBE0/def2-tzvp level.
(51) Warren, J. J.; Tronic, T. A.; Mayer, J. M. *Chem. Rev.* **2010**, *110*, 6961−7001.
(52) Hammes-Schiffer, S.; Stuchebrukhov, A. *Chem. Rev.* **2010**, *110*, 6939−6960.
(53) Layfield, J. P.; Hammes-Schiffer, S. *Chem. Rev.* **2014**, *114*, 3466−3494.
(54) Mullins, C. S.; Grapperhaus, C. A.; Kozlowski, P. M. *J. Biol. Inorg. Chem.* **2006**, *11*, 617−625.
(55) Herdt, D. R.; Grapperhaus, C. A. *Dalton Trans.* **2012**, *41*, 364−366.
(56) Green, K. N.; Brothers, S. M.; Jenkins, R. M.; Carson, C. E.; Grapperhaus, C. A.; Darensbourg, M. Y. *Inorg. Chem.* **2007**, *46*, 7536−7544.
(57) Bryngelson, P. A.; Arobo, S. E.; Pinkham, J. L.; Cabelli, D. E.; Maroney, M. J. *J. Am. Chem. Soc.* **2004**, *126*, 460−461.
(58) Pelmenschikov, V.; Siegbahn, P. E. M. *J. Am. Chem. Soc.* **2006**, *128*, 7466−7475.